Available online at www.sciencedirect.com
ScienceDirect
Geochimica et Cosmochimica Acta 72 (2008) 2349–2376
Geochimica et Cosmochimica Acta
www.elsevier.com/locate/gca

Recycled crust controls contrasting source compositions of Mesozoic and Cenozoic basalts in the North China Craton

Yongsheng Liu [a,b,*], Shan Gao [a,b], Peter B. Kelemen [c], Wenliang Xu [d]

[a] State Key Laboratory of Geological Processes and Mineral Resources, Faculty of Earth Sciences, China University of Geosciences, Wuhan 430074, China
[b] State Key Laboratory of Continental Dynamics, Department of Geology, Northwest University, Xi'an 710069, China
[c] Department of Earth and Environmental Sciences, Columbia University, NY 10964-8000, USA
[d] College of Earth Sciences, Jilin University, Changchun 130061, China

Received 1 October 2007; accepted in revised form 28 February 2008; available online 18 March 2008

Abstract

We explore Fe/Mn and Nb/Ta ratios of basalts as potential tracers for differentiating melts of recycled mafic crustal lithologies from peridotitic melts. Trace elements and Fe/Mn ratios of the Mesozoic and Cenozoic basalts from East China were analyzed by ICP-MS. Low Nb/Ta ratios (15.4 ± 0.3 (2σ, $n = 45$)), high Nb and Ta contents (60.1 and 4.01 ppm) and high Fe/Mn ratios (64.7 ± 1.5 (2σ, $n = 45$)) characterize the <110 Ma basalts. Mesozoic basalts with ages >110 Ma are characterized by superchondritic Nb/Ta ratios (20.1 ± 0.3 (2σ, $n = 25$)), low Nb and Ta contents (10.8 and 0.54 ppm) and slightly lower Fe/Mn ratios (60.0 ± 1.1 (2σ, $n = 25$)). Both the Mesozoic and Cenozoic basalts have Fe/Mn ratios higher than basaltic melt formed by partial melting of peridotite at the same MgO and CaO levels. Although both the Mesozoic and Cenozoic basalts are characterized by highly fractionated REE patterns, the >110 Ma basalts have island arc-type trace element patterns (i.e., depletion in Nb and Ta), whereas OIB-type trace element patterns (e.g., no depletion in Nb and Ta) are characteristic of the <110 Ma basalts. Based on $D_{Fe/Mn}$ values for olivine, clinopyroxene, orthopyroxene and garnet, high Fe/Mn ratios and negative correlations of Fe/Mn with Yb (Y) of the <110 Ma basalts suggest clinopyroxene/garnet-rich mantle sources. The lower Fe/Mn ratios and positive correlations of Fe/Mn with Y and Yb in the >110 Ma basalts suggest orthopyroxene/garnet-rich mantle sources. Combining these data with Sr–Nd isotopes, we present a conceptual model to explain the Nb/Ta ratios and PM-normalized trace element patterns of the >110 and <110 Ma basalts. Preferential melting of recycled ancient lower continental crust during Mesozoic lithospheric thinning resulted in (1) *peridotite-melt/fluid reaction that formed the orthopyroxene/garnet-rich mantle sources for the >110 Ma basalts*, and (2) *peridotite + rutile-bearing eclogite mixing that formed the clinopyroxene/garnet-rich mantle sources for the <110 Ma basalts*. The choice of models may indeed be arbitrary and non-unique, but the goal is to seek relatively simple forward models that explain the characteristics of the lavas, and the differences between the >110 and <110 Ma basalts, in a relatively consistent geodynamic framework.

1. INTRODUCTION

1.1. The ubiquity of garnet pyroxenite sources in the mantle

To the first order, the Earth's mantle is often thought as being largely peridotitic. Most of the volcanism on Earth is believed to have been generated by melting of peridotitic mantle. However, there are many reasons to think that the mantle may exhibit significant major-element heterogeneity and that such heterogeneities may strongly influence magmatism. We know that mafic crustal materials, such as oceanic crust or lower arc and continental crust, can be recycled back into the convecting mantle (Ringwood and Green, 1966), the former by subduction and the latter by foundering or delamination (Kay and Kay, 1991; Rudnick, 1995; Yuan et al., 2000;

* Corresponding author. Fax: +86 27 67885096.
E-mail addresses: yshliu@cug.edu.cn, yshliu@hotmail.com (Y. Liu).

0016-7037/$ - see front matter © 2008 Elsevier Ltd. All rights reserved.
doi:10.1016/j.gca.2008.02.018

Kelemen et al., 2003; Gao et al., 2004; Lustrino, 2005; Lee et al., 2006). Then, because of their lower melting points (at a given pressure) compared to peridotite (Yasuda et al., 1994; Hirschmann and Stolper, 1996; Hirschmann, 2000; Yaxley, 2000; Pertermann and Hirschmann, 2003b; Keshav et al., 2004; Kogiso et al., 2004), they could melt preferentially relative to peridotitic mantle to produce a high-Si liquid that is highly reactive with peridotite (Kelemen, 1986; Kelemen, 1995; Yaxley and Green, 1998; Rapp et al., 1999). As melt infiltrates the peridotite, it converts olivine to pyroxene, eventually forming an olivine-free pyroxenite (Rapp et al., 1999; Liu et al., 2005). Under conditions of local equilibrium, the olivine replacement forms a sharp reaction front, which advances into the peridotite to form garnet- and pyroxene-rich lenses in a peridotitic mantle (Sobolev et al., 2005).

How extensive are these chemical heterogeneities, and to what extent are mantle-derived magma compositions influenced by major-element heterogeneities? Although some have argued against the existence of garnet–pyroxenite or eclogite in the source of Hawaiian basalts (Stracke et al., 1999), for example, experimental studies and geochemical/petrological modeling suggest that pyroxenite/eclogite could be an important source component in some basaltic magmas (Allégre and Turcotte, 1986; Anderson, 1989; Hauri, 1996; Kogiso et al., 1998; Yaxley and Green, 1998; Korenaga and Kelemen, 2000; Lassiter et al., 2000; Salters and Dick, 2002; Meibom and Anderson, 2003; Hirschmann et al., 2003; Kogiso et al., 2003; Pertermann and Hirschmann, 2003b; Kogiso et al., 2004; Anderson, 2005; Sobolev et al., 2005; Gaffney et al., 2005; Anderson, 2006; Herzberg, 2006; Sobolev et al., 2007). Recycled basaltic material has been advocated to explain geochemical variability in mid-ocean ridge basalts (Hirschmann and Stolper, 1996; Eiler et al., 2000; Donnelly et al., 2004; Elliott et al., 2006), intraplate basalts (Kogiso et al., 1998; Lustrino et al., 2000; Niu and O'Hara, 2003; Kogiso et al., 2003; Lustrino and Dallai, 2003; Escrig et al., 2004; Lustrino, 2005; Sobolev et al., 2005; Lustrino et al., 2007), subduction-related magmas (Kay, 1978; Kelemen et al., 1993; Yogodzinski et al., 1995; Schiano et al., 2000) and flood basalts (Cordery et al., 1997; Yaxley, 2000). More recently, Sobolev et al. (2007) suggested that ~2% to 30% of recycled crust is involved in mantle melting to form mid-ocean ridge basalts, ocean island and continental basalts and komatiites.

Quantifying the importance of these chemical heterogeneities should be of immediate concern to geochemists and petrologists. For example, estimates of primary magma temperatures, which indirectly provide information on the thermal state of the mantle, are fundamentally linked to assumptions about the mantle source composition (i.e., peridotitic or pyroxenitic). Moreover, the lower melting temperatures of eclogite and pyroxenite have even led some to suggest that some intraplate volcanism is controlled by "eclogite" pods, and if so, might imply a fundamentally different sort of origin to hotspot volcanism than plumes (Cordery et al., 1997; Anderson, 2005; Foulger et al., 2005).

1.2. Distinguishing garnet pyroxenite from peridotite source regions

An important step towards resolving the proportion of garnet pyroxenite in the mantle source of magmas would be to find a means of fingerprinting melts of recycled mafic lithologies. Here, we explore Fe/Mn and Nb/Ta ratios of basalts as tracers that might differentiate melts of recycled mafic crustal lithologies from peridotitic melts. Based on the high Fe/Mn ratios of the Hawaiian basalt, Humayun et al. (2004) speculated that the lower mantle may be enriched in iron compared to the upper mantle, and attributed this iron enrichment to core-mantle interaction. Alternatively, recent studies by Sobolev et al. (2005) attributed the high Fe/Mn ratios of the Hawaiian basalts to melting of an olivine-free mantle source, such as a pyroxenite. Resolving the difference between these two hypotheses may rekindle an interest in first-series transition metals in the geosciences (Lee, 2004). Compilation of experimental results demonstrates that clinopyroxene (cpx), orthopyroxene (opx) and garnet (gar) generally have $D_{Fe/Mn} < 1$ $\left(\text{where } D_{Fe/Mn} = \frac{Fe^{min}/Fe^{melt}}{Mn^{min}/Mn^{melt}}\right)$ and olivine (ol) has $D_{Fe/Mn} > 1$ (Fig. 1a and b). No systematic influence of pressure on $D_{Fe/Mn}$ values was observed. Although Fe/Mn and MnO show a inverse correlation in melts produced from both peridotites and pyroxenites, suggesting that Mn is more incompatible than Fe, Fe/Mn ratios of pyroxenite melts are commonly higher than those of peridotite melts (Fig. 1d). High Fe/Mn (>60) basaltic melts can be produced by partial melting of pyroxenite while the degree of melting is less than 70% (Kogiso and Hirschmann, 2001; Pertermann and Hirschmann, 2003a; Keshav et al., 2004; Kogiso et al., 2004), or hydrous peridotite while the degree of melting is greater than 50% (Gaetani and Grove, 1998; Falloon and Danyushevsky, 2000; Parman and Grove, 2004) (Fig. 1c). Basaltic melts in equilibrium with dry peridotite (Fe/Mn of primitive mantle is ~58) mostly have Fe/Mn <60 (Fig. 1c) (Hirose and Kushiro, 1993; Baker and Stolper, 1994; Walter, 1998; Falloon and Danyushevsky, 2000; Pickering-Witter and Johnston, 2000; Schwab and Johnston, 2001; Wasylenki et al., 2003; Laporte et al., 2004) unless the source was previously depleted (i.e., harzburgite instead of lherzolite) (Lee, 2004) or MnO content of the melt is <0.12 wt% (insert of Fig. 1d). Most natural basalts have MnO $\geqslant$0.12 wt% (For example, proportions of samples with MnO <0.12 wt% is <2.7% for MORB (http://www.ldeo.columbia.edu/RidgePetDB) and <1.7% for OIB (http://georoc.mpch-mainz.gwdg.de/georoc/)). Thus, for less than 50% melting, high Fe/Mn ratios (>60) in "primitive" basalts may point to an eclogite/pyroxenite source, while lower values suggest a peridotite source.

Nb and Ta may also be useful tracers. During melting of typical mantle silicates, Nb and Ta were thought to behave as identical twins due to their similar cationic radii and valence state (Taylor and McLennan, 1985). However, Niu and Batiza (1997), Niu et al. (2002) and Niu (2004) showed that Nb significantly fractionates from Ta in some basalts. Experiments have demonstrated that Nb and Ta fractionate when Ti-oxide phases, such as rutile, ilmenite and sphene,

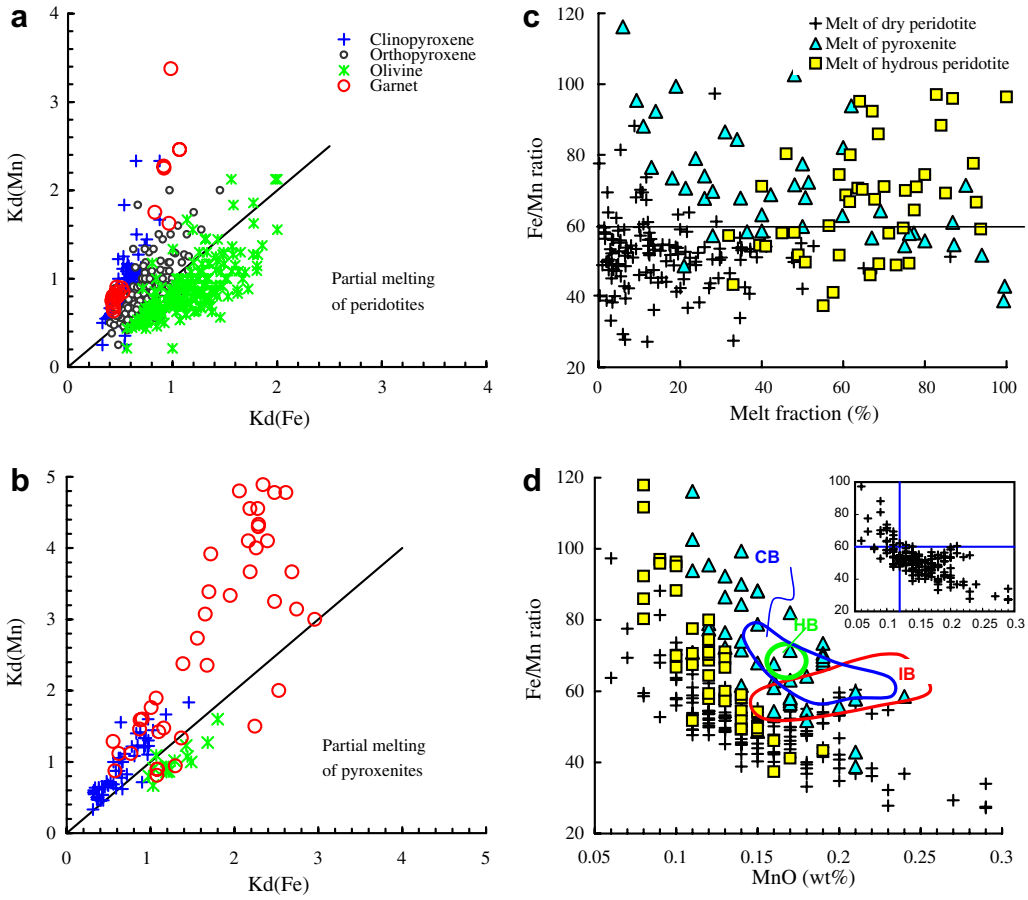

Fig. 1. (a and b) Plots of D_{Fe} vs. D_{Mn} for olivine, clinopyroxene, orthopyroxene and garnet during partial melting of peridotite and pyroxenite. *Peridotite*: cpx, opx and ol: (Baker and Stolper, 1994; Gaetani and Grove, 1998; Walter, 1998; Falloon et al., 1999; Pickering-Witter and Johnston, 2000; Falloon and Danyushevsky, 2000; Schwab and Johnston, 2001; Wasylenki et al., 2003; Laporte et al., 2004; Parman and Grove, 2004); gar: (Gaetani and Grove, 1998; Walter, 1998). *Pyroxenite*: cpx and gar: (Kogiso and Hirschmann, 2001; Kogiso et al., 2003; Pertermann and Hirschmann, 2003a; Keshav et al., 2004; Pertermann et al., 2004; Kogiso and Hirschmann, 2006); ol: (Kogiso and Hirschmann, 2001). (c, d) Plots of Fe/Mn ratios vs. melt fractions and MnO contents of basaltic melts formed by partial melting of pyroxenites (Kogiso and Hirschmann, 2001; Pertermann and Hirschmann, 2003a; Keshav et al., 2004; Kogiso et al., 2004), dry peridotites (Hirose and Kushiro, 1993; Baker and Stolper, 1994; Walter, 1998; Falloon and Danyushevsky, 2000; Pickering-Witter and Johnston, 2000; Schwab and Johnston, 2001; Wasylenki et al., 2003; Laporte et al., 2004) and hydrous peridotites (Gaetani and Grove, 1998; Falloon and Danyushevsky, 2000; Laporte et al., 2004; Parman and Grove, 2004). Products of melt–peridotite reaction (e.g., Falloon and Danyushevsky, 2000) and melts of high Fe/Mn peridotitic material (e.g., HK66; Hirose and Kushiro, 1993) were not compiled in (d). CB, HB and IB in (d) are ranges of <110 Ma basalts from Eastern China, Hawaiian basalts (Humayun et al., 2004) and Iceland basalts (Thomas Find et al., 2006), respectively.

are involved in melting or crystal fractionation ($D_{Nb}/D_{Ta}^{rutile/melt}$=0.21–1.0) (Green and Pearson, 1987; Klemme et al., 2005; and references therein). Not only does rutile strongly partition Nb and Ta ($D_{Nb,\,Ta}^{rutile/melt} \gg 1$), but rutile also effectively fractionates Nb from Ta, such that melts in equilibrium with rutile are characterized by high Nb/Ta ratios (Ryerson and Watson, 1987; Wendlandt, 1990; Ayers and Watson, 1991; Foley et al., 2000; Klemme et al., 2002; Klemme et al., 2005; Xiong et al., 2005). Both natural samples (Rudnick et al., 2000; Zhang et al., 2000; Xu et al., 2004; Jacob, 2004; Lee et al., 2006; Xu et al., 2006) and experimental products (Rapp and Watson, 1995; Kogiso et al., 1997; Rapp et al., 1999; Pertermann and Hirschmann, 2003a; Dasgupta et al., 2004; Xiong et al., 2005) indicate that rutile is a common mineral phase in eclogite/garnet–clinopyroxenite. Stability of rutile, however, during partial melting of basaltic compositions depends strongly on pressure, temperature, and perhaps H_2O content as well. Experiments indicate that rutile is stable on the basalt solidus but unstable (e.g., dissolved in melt or in silicate minerals) when the temperature exceeds ~1250 °C at 2.0–3.0 GPa (Klemme et al., 2002; Xiong et al., 2005). In summary, initial melts of rutile-bearing eclogite should have relatively high Nb/Ta ratios. Progressive melting of these eclogites would exhaust rutile, thereby resulting in melts with low Nb/Ta ratios inherited from earlier melt depletion. By contrast, melts of rutile-free peridotitic mantle would be characterized by Nb/Ta ratios close to the primitive mantle value if the peridotitic mantle source was not affected by recycled crust.

1.3. Case studies of basalts in the North China craton

To apply these concepts, we turn to the eastern block of the North China Craton (NCC), where the Archaean craton is believed to have lost its lithospheric keel (Menzies et al., 1993; Griffin et al., 1998; Menzies and Xu, 1998; Gao et al., 2002; Wu et al., 2003; Menzies et al., 2007). Our previous studies of high-Mg# intermediate to felsic lavas from western Liaoning suggest that recycling of components from Archean lower crustal eclogite via partial melting occurred beneath the NCC during the Early Mesozoic (Gao et al., 2004; Xu et al., 2006). In addition to the Mesozoic basalts accompanying lithospheric thinning/removal, abundant Cenozoic basalts of varying age occur in this region.

The >110 Ma basalts (Pei et al., 2004; Yang et al., 2004; Zhang et al., 2004; Gao et al., 2008) and underplated mafic magma (e.g., the Hannuoba lower crustal xenoliths; Liu et al., 2001; Zhou et al., 2002; Liu et al., 2004) were characterized by EMI and/or EMII-type Nd and Sr isotopic compositions and island arc-type trace element patterns. The <110 Ma basalts have relatively depleted Nd and Sr isotopic compositions and ocean island basalt (OIB)-type trace element patterns (Zhou and Armstrong, 1982; Zhi et al., 1990; Liu et al., 1995a; Hsu and Chen, 1998; Zou et al., 2000; Zhang and Zheng, 2003; Xu et al., 2005). To interpret the contrasting characteristics of the >110 and <110 Ma basalts, partial melting of ancient subducted lithosphere (Zhou et al., 2001), ancient subduction-related metasomatic lithospheric mantle (Zhang et al., 2002; Zhang et al., 2003), or contamination by continental crust (Xie et al., 2001; Xu and Xie, 2005) have been advocated for the >110 Ma basalts, while the <110 Ma basalts were thought to be derived from eclogite component-bearing mantle or veined garnet pyroxenite–garnet lherzolite mantle (Zhi et al., 1990), metasomatized mantle with EMI feature (Hsu and Chen, 1998), mixture of asthenospheric mantle and EMI or EMII components (Zou et al., 2000), or refractory peridotites metasomatized by garnet lherzolite melts (Xu et al., 2005).

Common presence of high-Mg# adakitic lavas in East China suggests that mafic lower continental crust was recycled into the convecting mantle during the Mesozoic lithospheric thinning (Xu et al., 2002; Gao et al., 2004; Xu et al., 2008), which could have resulted in (1) silicic melt–peridotite reaction by equilibrium infiltration, (2) mechanical mixing of peridotite and silicic melt by injection and freezing of melts into cold lithospheric mantle, and (3) solid-state mechanical mixing of peridotite and the eclogitic residues after silicic melt extraction. Here, we present precise measurements of Fe/Mn and Nb/Ta in the Mesozoic and Cenozoic basalts from East China. Our results show that melting of a peridotite + rutile-bearing eclogite mixture could explain the formation of OIB-type features of the <110 Ma basalts, and lithospheric mantle metasomatized by rutile-bearing eclogite-derived melts could be an important source for the >110 Ma basalts.

2. GEOLOGICAL SETTING

The North China Craton (NCC) is one of the world's oldest cratons. The presence of $\geqslant$3.6 Ga crustal remnants exposed at the surface and in lower crustal xenoliths in both the northern and southern parts of the craton suggests that it has remained partially intact since the early Archean (Liu et al., 1992a; Zheng et al., 2004). Based on age, lithological assemblage, tectonic evolution and *P–T–t* paths, the NCC can be divided into the Eastern Block, the Western Block and the intervening Trans-North China Orogen (Fig. 2) (Zhao et al., 2000). The craton is believed to have experienced widespread tectonothermal reactivation during the Late Mesozoic and Cenozoic based on high surface heat flow, voluminous Late Mesozoic magmatism, uplift and later basin development, slow seismic wave speeds in the upper mantle, present-day strong seismicity, and a change in the character of mantle xenoliths sampled by Paleozoic to Cenozoic magmas. Collectively, these observations have been used to suggest that ancient, cratonic mantle lithosphere, similar to that presently beneath the Kaapvaal, Siberian and other Archean cratons, was removed from the base of the eastern block of the NCC sometime after the Ordovician, and replaced by younger, less refractory mantle (Menzies et al., 1993; Griffin et al., 1998; Gao et al., 2002; Wu et al., 2003; Gao et al., 2004; Rudnick et al., 2004; Wu et al., 2006; Menzies et al., 2007).

3. SAMPLES AND ANALYTICAL METHODS

One hundred and eight basalt samples from the NCC were analyzed in this work. The basalts analyzed in this work are summarized in Fig. 2. The >110 Ma basalts show porphyritic texture and massive structure, and consist of 2–15% phenocrysts of olivine, clinopyroxene and minor orthopyroxene (Zhang et al., 2002; Pei et al., 2004). F_o values of olivine cores are mostly >90 (Pei et al., 2004; Gao et al., 2008). Detailed petrologic and mineral chemical studies by Gao et al. (2008) indicate that these basalts represent primary melts derived from pyroxenite sources. The <110 Ma basalts show porphyritic texture and massive structure, most of which consist of fewer phenocrysts of olivine and pyroxene. Unlike the >110 Ma basalts, olivine phenocrysts in the <110 Ma basalts have lower F_o values (50–90) (Chi, 1987).

All samples were crushed in a corundum jaw crusher (to 60 mesh). About 60 g was powdered in an agate ring mill to less than 200 mesh. The samples were digested by HF + HNO_3 in Teflon bombs and analyzed with an Agilent 7500a ICP-MS at the China University of Geosciences. Fe/Mn ratios were determined with standard solutions of Fe and Mn as described by Humayun et al. (2004). The standard solutions with 50 ppb Mn and 2–4 ppm Fe were prepared gravimetrically by combining high-purity Mn and Fe solutions with Fe/Mn ratios in the range of 40–80. Interferences from argon-based polyatomic ions were corrected by subtracting the ^{57}Fe and ^{55}Mn counts from a 2% HNO_3 solution. Internal standard (^{115}In)-normalized signal/background ratios are $>10^3$ for both ^{57}Fe and ^{55}Mn (production of $^{40}Ca^{17}O$ and $^{39}K^{16}O$ was negligible). The Fe/Mn ratios of the samples were calibrated using BHVO-1 with Fe/Mn = 65.7 (total Fe_2O_3 = 12.23 wt%, MnO = 0.168 wt%; http://georem.mpch-mainz.gwdg.de).

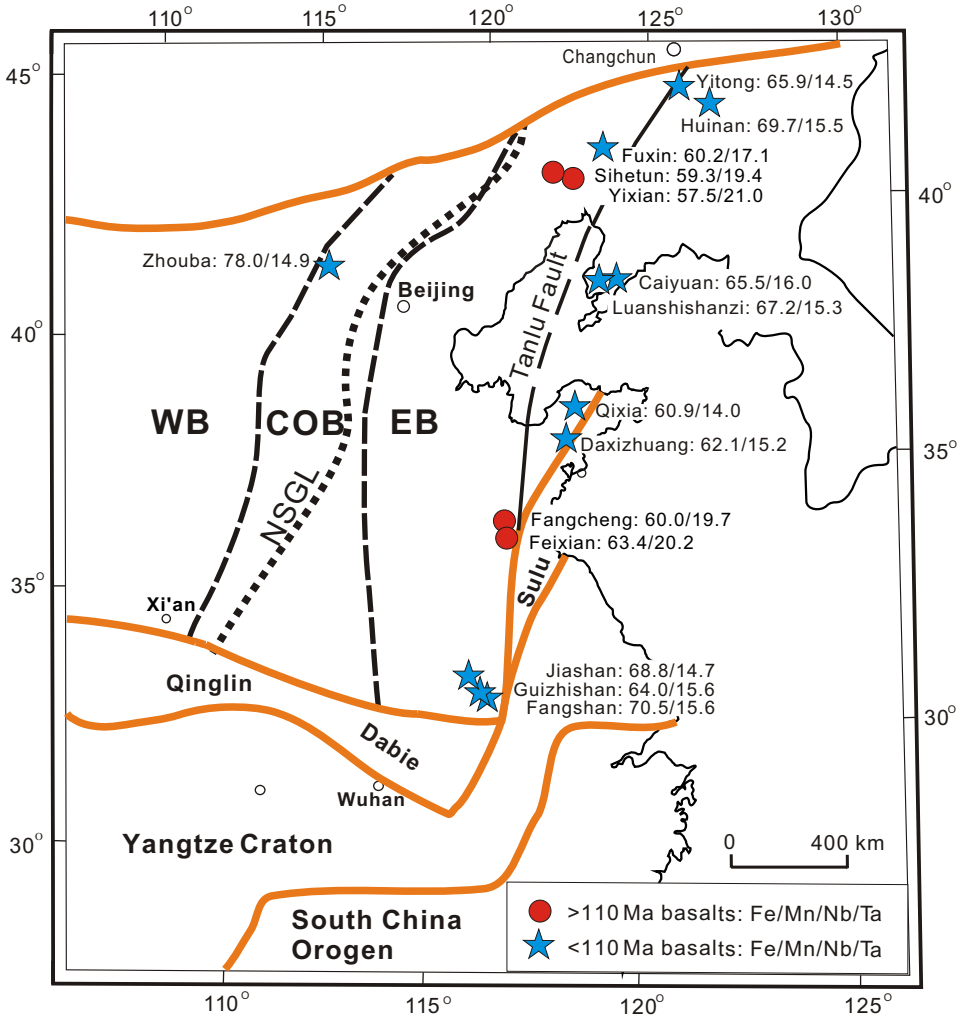

Fig. 2. Sampling locations and summary of Fe/Mn and Nb/Ta ratios of the basalts in this study.

Analyses of BCR-2 and BHVO-2 give Fe/Mn ratios of 63.3 ± 0.2 (2σ, $n = 4$) and 66.4 ± 0.3 (2σ, $n = 4$), respectively. These are comparable to calculated Fe/Mn ratios of 63.5 and 66.7 for BCR-2 and BHVO-2, respectively, according to the recommended Fe and Mn contents. Our measured Fe/Mn ratio of BHVO-2 agrees well with the value (66.1) obtained by Humayun et al. (2004). Similarly, Nb/Ta ratios of the basalts were calibrated by standard solutions of Nb and Ta with Nb/Ta ratios ranging from 10 to 30. Analyses of BCR-2, BHVO-1 and BHVO-2 give Nb/Ta ratios of 16.2 ± 0.6 (2σ, $n = 4$), 15.2 ± 0.4 (2σ, $n = 4$) and 15.2 ± 0.2 (2σ, $n = 4$), respectively. The Nb/Ta ratios obtained for BHVO-1 and BHVO-2 in this study are consistent with those determined by isotope dilution (15.1–15.4) by Pfänder et al. (2007).

4. RESULTS

In order to reduce the possibility of crystal fractionation involving oxides or clinopyroxene, both affecting Fe/Mn ratios and the former affecting Nb/Ta ratios, a subset of 45 Mesozoic and 37 Cenozoic basalt samples with MgO >7.5 wt% were selected for this study (Table 1). The >110 Ma basalts have SiO_2, MgO and total Fe_2O_3 compositions overlapping with partial melts of peridotite, but lower CaO contents (Fig. 3). The <110 Ma basalts have higher total Fe_2O_3 and TiO_2 contents. Their MgO–SiO_2, –CaO and —total Fe_2O_3, and CaO—total Fe_2O_3 variations are similar to partial melts of pyroxenite.

The Mesozoic and Cenozoic basalts have trace element signatures (e.g., low heavy rare-earth element (HREE) contents and high La/Yb ratios) suggesting the involvement of residual garnet in their formation (Fig. 4). The >110 Ma basalts are characterized by high Zr/Nb ratios (15.4–18.8) (Table 1), low Nb and Ta contents, notable Nb and Ta depletions relative to Th and La, and positive or non-existent Pb anomalies relative to Ce, all of which are features commonly seen in arc lavas. Nb, Ta, Yb and Y correlate negatively with MgO (Fig. 5a–d). Most of them have high Ni (217–505 ppm) and Cr (519–1368 ppm) contents (Fig. 5c and f). Except for Pb, the <110 Ma basalts have HIMU-OIB-type trace element patterns (e.g., no depletion

Table 1
Chemical compositions and Fe/Mn and Nb/Ta ratios of the basalts

Location	Feixian, Shandong							Fangcheng Shandong					
Age	(119 Ma; Pei et al., 2004)							(124.9 Ma; Zhang et al., 2002)					
Sample	SFX02	SFX13	SFX19	SFX27	SFX28	SFX30	SFX-49	SFC05	SFC06	SFC09	SFC14	SFC17	SFC31
SiO_2	48.8	48.6	48.7	49.2	49.5	48.9	48.5	47.8	48.0	48.1	47.3	48.0	48.0
TiO_2	1.09	1.10	1.10	1.07	1.07	1.08	1.13	1.10	1.10	1.09	1.14	1.08	1.11
Al_2O_3	12.1	11.8	12.0	11.9	11.9	11.7	11.7	12.8	13.1	13.2	12.8	12.4	13.1
Fe_2O_{3total}	8.94	8.85	8.86	8.75	8.74	8.92	8.95	9.08	9.00	9.01	8.93	9.01	9.03
MnO	0.12	0.12	0.12	0.12	0.12	0.12	0.12	0.13	0.13	0.13	0.13	0.13	0.13
MgO	12.7	13.6	13.4	13.0	13.1	13.6	13.6	11.7	11.2	11.0	11.5	12.0	11.3
CaO	8.82	8.78	8.79	8.74	8.76	8.84	8.87	9.15	8.70	9.16	9.01	9.30	8.98
Na_2O	2.37	1.93	2.23	2.18	2.19	2.43	2.05	3.15	2.99	3.17	3.19	3.69	3.23
K_2O	2.29	2.62	2.62	2.72	2.53	2.08	2.24	1.15	1.36	1.22	1.03	1.14	1.23
P_2O_5	0.68	0.66	0.64	0.64	0.65	0.65	0.68	0.80	0.83	0.83	0.78	0.78	0.83
LOI	1.52	1.48	1.44	0.94	1.07	1.47	2.09	2.97	3.16	3.09	3.82	2.52	3.03
Total	99.4	99.5	99.9	99.3	99.5	99.8	99.8	99.9	99.7	99.9	99.6	99.9	100.0
Mg#	74.0	75.5	75.2	74.8	74.9	75.3	75.2	72.1	71.4	70.9	72.1	72.6	71.4
Be	1.68	1.73	1.55	1.63	1.61	1.64	1.74	1.59	1.70	1.75	1.71	1.69	1.73
Sc	20.7	20.6	20.2	20.8	20.5	20.6	20.5	21.5	20.9	21.5	22.0	21.3	20.7
V	157	151	151	152	150	154	157	162	160	162	164	163	159
Cr	609	703	681	667	671	675	663	590	519	573	534	568	539
Co	44.3	46.7	46.3	45.0	45.3	46.1	45.8	39.4	37.6	40.0	39.3	40.2	38.0
Ni	369	431	435	397	406	429	409	251	217	255	239	256	228
Cu	43.6	39.3	40.7	40.0	42.7	44.3	40.0	21.8	19.2	21.5	29.4	23.7	20.1
Zn	96.4	93.6	94.3	93.3	93.0	95.3	119	95.8	98.1	99.5	96.2	101	96.5
Ga	87.0	84.2	80.3	83.3	82.7	82.8	86.8	59.3	60.9	59.5	63.6	58.8	59.6
Rb	42.3	49.1	43.8	50.9	26.9	36.3	47.8	16.7	18.0	16.7	17.5	22.2	16.9
Sr	1506	1423	1393	1443	1440	1410	1539	1301	1378	1351	1360	1426	1292
Y	24.8	23.4	24.1	24.0	23.6	24.2	25.0	25.7	26.5	26.4	25.8	27.0	25.9
Zr	229	216	217	229	218	223	226	255	268	259	256	264	262
Nb	12.5	12.0	12.0	12.2	12.0	12.3	12.6	14.8	15.4	14.9	14.4	15.2	16.0
Cs	12.6	8.76	13.8	3.59	2.20	17.3	9.95	3.32	2.67	2.68	0.83	0.96	2.60
Ba	1948	1853	1801	1826	1834	1831	1691	1278	1316	1309	1359	1245	1210
La	93.0	86.9	86.7	87.3	85.6	88.2	93.1	106	107	106	101	105	106
Ce	181	171	168	170	168	169	184	203	211	209	199	209	206
Pr	25.2	23.6	23.6	23.7	23.5	24.0	25.4	28.6	28.8	28.9	27.6	28.8	28.6
Nd	93.8	88.8	88.5	88.7	87.9	89.7	94.6	104	105	105	101	105	104
Sm	15.1	14.3	14.3	14.1	14.3	14.7	15.0	15.4	15.3	15.5	15.1	15.3	15.3
Eu	4.11	3.98	3.89	3.91	3.88	3.99	4.22	3.84	3.87	3.89	3.86	3.92	3.85
Gd	11.7	11.2	11.1	11.0	11.0	11.3	11.8	11.4	11.2	11.2	11.2	11.4	11.3
Tb	1.22	1.13	1.15	1.16	1.15	1.17	1.20	1.20	1.20	1.19	1.18	1.20	1.20
Dy	5.23	4.99	4.96	5.05	4.95	5.08	5.22	5.31	5.38	5.34	5.27	5.34	5.27
Ho	0.84	0.80	0.82	0.84	0.80	0.83	0.85	0.89	0.89	0.90	0.88	0.90	0.88
Er	2.14	2.04	2.04	2.07	2.02	2.10	2.11	2.27	2.31	2.25	2.27	2.36	2.28
Tm	0.28	0.26	0.28	0.27	0.26	0.28	0.28	0.30	0.32	0.30	0.30	0.31	0.31
Yb	1.57	1.54	1.50	1.56	1.56	1.52	1.58	1.76	1.85	1.80	1.73	1.83	1.80
Lu	0.23	0.23	0.24	0.23	0.22	0.23	0.24	0.27	0.26	0.26	0.26	0.27	0.27
Hf	5.02	4.79	4.85	5.10	4.85	4.93	4.98	5.48	5.80	5.56	5.59	5.66	5.64
Ta	0.61	0.59	0.60	0.61	0.60	0.61	0.61	0.75	0.78	0.75	0.75	0.77	0.82
Pb	17.8	16.1	16.8	18.1	17.5	17.6	18.0	16.9	17.7	16.8	16.0	17.2	17.0
Th	11.4	10.9	10.6	11.0	10.9	10.8	11.5	11.2	11.7	11.3	10.9	11.6	11.4
U	1.64	1.58	1.53	1.60	1.57	1.57	1.64	1.78	1.92	1.81	1.76	1.87	1.85
Zr/Nb	18.4	18.0	18.1	18.8	18.2	18.0	18.0	17.2	17.4	17.3	17.8	17.3	16.4
Nb/Ta	20.4	20.3	20.1	19.9	19.9	20.1	20.5	19.8	19.7	19.8	19.3	19.9	19.5
Fe/Mn[a]	64.2	63.2	63.7	62.6	62.6	63.4	63.5	60.1	60.0	59.4	60.2	60.1	59.7
2σ	0.62	0.53	0.41	0.46	0.54	0.86	0.50	0.37	0.67	0.46	0.71	0.87	0.42
Fe/Mn[b]	67.3	66.6	66.7	65.8	65.8	67.1	67.4	63.1	62.5	62.6	62.0	62.6	62.7

Location	Sihetun, Liaoning						Yixian, Liaoning					
Age	(124-125 Ma; Gao et al., 2008)						(122-125 Ma; Zhou et al., 2003)					
Sample	SHT-16	SHT-19	SHT-21	SHT-24	SHT-28	SHT-31	YX-25	YX-26	YX-27	YX-30	YX-103	YX-108
SiO_2	49.9	49.8	49.4	50.2	50.2	50.5	49.3	48.9	49.3	49.6	49.3	49.3
TiO_2	0.86	0.84	0.84	0.82	0.83	0.87	0.71	0.69	0.71	0.73	0.70	0.70

Table 1 (*continued*)

Location	Sihetun, Liaoning						Yixian, Liaoning					
Age	(124-125 Ma; Gao et al., 2008)						(122-125 Ma; Zhou et al., 2003)					
Sample	SHT-16	SHT-19	SHT-21	SHT-24	SHT-28	SHT-31	YX-25	YX-26	YX-27	YX-30	YX-103	YX-108
Al_2O_3	12.6	13.0	12.7	12.0	12.8	12.9	12.5	12.4	12.5	12.5	12.3	12.4
Fe_2O_{3total}	8.40	8.53	8.48	8.31	8.53	8.36	9.59	9.56	9.51	9.14	9.47	9.41
MnO	0.12	0.11	0.12	0.13	0.11	0.12	0.14	0.14	0.14	0.14	0.15	0.15
MgO	12.3	11.0	11.1	11.9	10.9	11.5	14.1	14.4	13.9	12.8	14.0	14.0
CaO	7.30	7.83	8.08	7.18	8.14	7.32	7.57	7.44	7.46	7.59	7.48	7.30
Na_2O	2.69	2.52	2.48	2.68	2.58	3.01	2.99	2.89	2.98	3.25	3.13	2.99
K_2O	2.30	2.44	2.35	3.12	2.39	2.35	1.27	1.22	1.26	1.45	1.27	1.29
P_2O_5	0.67	0.80	0.77	0.73	0.77	0.67	0.68	0.66	0.67	0.68	0.67	0.67
LOI	2.39	2.68	3.25	2.65	2.33	2.14	1.57	1.84	1.76	1.75	1.19	2.08
Total	99.5	99.6	99.5	99.7	99.5	99.7	100	100	100	99.6	99.6	100
Mg#	74.5	72.1	72.3	74.1	71.8	73.4	74.6	75.1	74.5	73.7	74.7	74.8
Be	1.71	2.05	2.02	1.73	1.98	2.00	1.29	1.29	1.27	1.40	1.29	1.37
Sc	21.3	25.4	24.8	22.5	25.3	25.7	27.9	28.3	27.6	26.5	27.6	28.2
V	145	173	170	153	174	179	196	191	191	191	193	197
Cr	1164	958	851	981	826	812	1368	1318	1351	969	1308	1270
Co	53.8	43.8	42.2	47.4	42.4	41.0	51.8	51.2	52.8	46.2	52.6	50.4
Ni	505	273	270	375	253	237	376	376	389	294	396	354
Cu	46.9	53.6	58.4	48.1	63.9	43.7	71.7	71.3	76.4	62.2	77.2	71.2
Zn	79.3	78.8	76.2	78.0	79.1	78.5	79.6	78.6	79.9	77.9	79.7	75.9
Ga	52.6	64.3	63.4	56.3	68.0	68.7	28.1	28.0	28.6	32.3	28.3	29.2
Rb	50.9	55.3	55.5	55.8	57.7	58.8	25.0	23.9	24.0	26.7	24.8	26.0
Sr	610	742	756	651	804	800	598	594	601	718	609	609
Y	19.2	22.6	22.3	20.3	23.0	23.3	13.1	13.3	12.9	13.3	13.4	13.2
Zr	138	144	154	150	143	152	104	103	102	115	106	108
Nb	8.46	8.55	8.67	9.12	8.61	8.79	6.63	6.52	6.52	7.49	6.68	6.81
Cs	2.45	2.58	2.58	2.74	2.55	2.55	2.39	2.58	2.19	1.60	2.05	2.80
Ba	1045	1333	1299	1066	1326	1321	483	491	502	586	485	492
La	45.6	55.9	56.7	47.8	59.1	59.8	16.0	15.8	15.5	18.0	15.9	16.3
Ce	85.3	106	107	90.7	110	112	34.9	34.6	34.1	39.4	34.9	35.3
Pr	12.3	15.3	15.5	12.8	16.1	16.3	4.48	4.40	4.32	4.93	4.41	4.55
Nd	49.5	61.4	62.0	51.3	64.3	65.0	17.9	17.7	17.3	19.6	17.7	18.3
Sm	9.76	12.1	12.0	9.92	12.4	12.6	3.31	3.21	3.24	3.50	3.35	3.32
Eu	2.72	3.38	3.35	2.83	3.53	3.51	1.05	1.04	1.04	1.14	1.03	1.08
Gd	7.93	9.66	9.72	8.19	10.2	10.3	3.12	3.09	3.03	3.30	3.13	3.17
Tb	0.89	1.08	1.08	0.91	1.11	1.13	0.41	0.41	0.41	0.42	0.42	0.44
Dy	4.08	4.78	4.85	4.18	4.99	5.05	2.36	2.31	2.25	2.40	2.31	2.33
Ho	0.66	0.76	0.74	0.67	0.80	0.79	0.45	0.45	0.45	0.45	0.45	0.47
Er	1.61	1.87	1.86	1.71	1.96	1.92	1.27	1.26	1.25	1.20	1.25	1.28
Tm	0.22	0.25	0.25	0.22	0.25	0.26	0.19	0.19	0.18	0.18	0.19	0.20
Yb	1.28	1.41	1.39	1.37	1.49	1.45	1.15	1.13	1.16	1.12	1.10	1.16
Lu	0.19	0.21	0.21	0.20	0.20	0.22	0.17	0.18	0.17	0.18	0.18	0.18
Hf	3.11	3.42	3.45	3.31	3.22	3.43	2.31	2.26	2.26	2.51	2.34	2.37
Ta	0.45	0.43	0.43	0.49	0.44	0.45	0.32	0.31	0.31	0.35	0.32	0.33
Pb	14.4	17.3	17.1	15.4	17.7	17.9	13.5	13.2	13.1	14.4	13.5	13.9
Th	6.04	7.19	7.21	6.36	7.50	7.51	1.50	1.43	1.43	1.69	1.51	1.51
U	1.12	1.14	1.36	1.18	1.43	1.46	0.38	0.38	0.37	0.44	0.40	0.41
Zr/Nb	16.3	16.8	17.7	16.4	16.6	17.3	15.7	15.7	15.7	15.4	15.8	15.9
Nb/Ta	18.8	19.8	20.0	18.5	19.8	19.6	20.7	20.8	21.3	21.2	20.9	20.9
Fe/Mn[a]	56.9	60.0	57.4	61.2	61.0	54.5	58.1	57.8	58.3	56.0	57.8	58.0
2σ	0.44	0.48	0.86	0.64	0.73	0.47	0.73	0.35	0.57	0.41	0.60	0.47
Fe/Mn[b]	63.2	70.0	63.8	59.6	70.0	62.9	61.9	61.7	61.3	59.0	57.0	56.7
Location	Fuxin, Liaoning						Qujiatun, Liaoning				Luanshishanzi, Liaoning	
Age	(100.4 Ma; Zhang and Zheng, 2003)						(81.6 Ma; Wang et al., 2006)				(58.4 Ma; Wang et al., 2006)	
Sample	JG-3	JG-4	JG-5	JG-6	JG-35	JG-37	DD19-1	DD19-2	DD19-2	DD19-3	DD18-1	DD18-4
SiO_2	44.0	44.1	44.1	44.2	44.1	44.0	44.0	43.7	43.7	43.5	45.6	45.3
TiO_2	2.94	2.89	2.97	2.91	2.95	2.94	2.57	2.58	2.58	2.64	2.49	2.28

(*continued on next page*)

Table 1 (*continued*)

Location	Fuxin, Liaoning						Qujiatun, Liaoning				Luanshishanzi, Liaoning	
Age	(100.4 Ma; Zhang and Zheng, 2003)						(81.6 Ma; Wang et al., 2006)				(58.4 Ma; Wang et al., 2006)	
Sample	JG-3	JG-4	JG-5	JG-6	JG-35	JG-37	DD19-1	DD19-2	DD19-2	DD19-3	DD18-1	DD18-4
Al_2O_3	15.0	14.9	15.0	15.0	15.1	14.9	14.0	14.1	14.1	13.5	11.7	10.6
Fe_2O_{3total}	12.0	11.9	12.1	11.9	12.0	12.0	13.7	13.7	13.7	13.7	12.9	13.2
MnO	0.18	0.18	0.18	0.18	0.18	0.18	0.20	0.20	0.20	0.20	0.17	0.18
MgO	8.44	8.65	8.42	8.54	8.47	8.68	7.87	7.86	7.86	8.82	12.8	14.3
CaO	10.1	10.0	10.2	10.1	10.1	9.88	12.4	12.4	12.4	12.6	10.4	10.4
Na_2O	2.97	3.22	2.91	3.07	2.96	2.93	2.45	2.61	2.61	2.42	2.31	2.12
K_2O	1.93	2.07	1.98	1.99	1.93	1.98	1.02	0.87	0.87	0.89	0.80	0.71
P_2O_5	0.62	0.63	0.62	0.62	0.62	0.62	0.59	0.60	0.60	0.56	0.45	0.42
LOI	1.46	0.97	1.44	1.34	1.14	1.53	1.84	1.98	1.98	1.83	1.14	1.29
Total	99.7	99.6	99.8	99.9	99.5	99.6	101	101	101	101	101	101
Mg#	58.5	59.2	58.3	58.9	58.6	59.2	53.5	53.4	53.4	56.4	66.5	68.4
Be	2.10	2.27	2.11	2.08	2.25	2.15	1.12	1.02	1.23	1.22	0.94	0.94
Sc	27.5	27.6	27.1	25.0	25.8	25.6	32.2	31.5	31.6	33.8	24.5	27.4
V	313	286	292	324	274	255	339	326	347	340	211	213
Cr	265	255	253	279	236	223	163	151	160	248	690	850
Co	60.7	58.6	60.6	57.7	56.0	54.8	46.6	44.9	47.6	48.5	58.4	66.3
Ni	168	169	163	173	159	156	67.0	64.3	70.4	89.3	351	416
Cu	69.2	69.9	70.9	67.1	72.4	67.5	60.5	63.5	67.3	80.4	47.8	49.7
Zn	103	105	103	103	103	103	108	104	109	104	98.9	101
Ga	20.6	21.0	20.4	20.1	20.4	20.4	21.2	20.5	21.7	20.7	16.9	16.4
Rb	51.0	52.0	50.0	48.0	51.0	50.0	20.9	14.9	16.0	23.3	14.4	14.1
Sr	806	757	763	766	869	786	1036	1001	1072	887	492	458
Y	26.0	26.0	26.0	27.0	27.0	27.0	26.0	25.0	26.3	25.3	23.6	23.1
Zr	251	253	241	238	237	240	295	283	299	277	198	190
Nb	69.5	69.3	68.0	67.3	66.1	67.3	49.6	47.5	50.6	46.1	24.4	23.5
Cs	0.45	0.52	0.49	0.58	0.52	0.64	0.41	0.40	0.41	0.40	0.41	0.48
Ba	813	829	786	792	795	793	425	410	437	386	228	215
La	43.7	44.4	42.6	42.3	42.0	42.5	41.4	39.9	42.1	37.7	19.4	18.4
Ce	86.7	86.0	83.9	83.4	81.8	83.0	92.6	88.9	94.3	85.2	44.4	42.0
Pr	10.5	10.8	10.6	10.3	10.3	10.6	12.1	11.7	12.6	11.4	6.17	5.84
Nd	41.9	42.9	41.8	40.8	40.0	42.3	52.4	50.7	53.8	49.5	28.4	27.2
Sm	8.32	8.42	8.22	8.08	8.17	8.61	10.5	10.0	10.5	9.91	6.97	6.87
Eu	2.61	2.66	2.63	2.56	2.55	2.62	3.04	2.93	3.12	2.96	2.20	2.15
Gd	7.94	7.95	7.87	7.72	7.82	7.96	8.45	8.05	8.48	8.05	6.46	6.33
Tb	1.03	1.09	1.06	1.03	1.05	1.09	1.11	1.08	1.13	1.09	0.96	0.93
Dy	5.57	5.63	5.45	5.34	5.38	5.53	5.80	5.47	5.79	5.68	5.24	5.12
Ho	1.04	1.06	1.03	1.02	1.02	1.05	1.00	0.97	1.04	1.00	0.93	0.88
Er	2.68	2.74	2.68	2.61	2.61	2.73	2.60	2.46	2.56	2.46	2.26	2.23
Tm	0.36	0.36	0.36	0.35	0.36	0.38	0.32	0.31	0.34	0.31	0.30	0.29
Yb	2.36	2.39	2.34	2.31	2.27	2.35	1.97	1.87	2.06	1.99	1.73	1.67
Lu	0.36	0.36	0.36	0.34	0.34	0.37	0.29	0.26	0.28	0.28	0.23	0.22
Hf	5.65	5.86	5.64	5.55	5.26	5.60	6.73	6.29	6.65	6.33	4.62	4.52
Ta	4.31	4.29	4.22	4.17	4.00	4.30	3.80	2.87	3.08	2.87	1.58	1.54
Pb	3.77	4.08	3.77	3.81	4.00	3.82	3.90	3.92	4.11	1.38	2.48	2.44
Th	5.29	5.42	5.11	5.00	5.02	4.73	4.27	4.12	4.31	3.79	1.98	1.90
U	1.46	1.50	1.49	1.39	1.45	1.42	1.26	1.21	1.28	1.11	0.57	0.54
Zr/Nb	3.60	3.65	3.55	3.54	3.59	3.56	5.94	5.96	5.91	6.01	8.12	8.10
Nb/Ta	17.0	17.2	17.2	17.4	16.8	17.0	13.1	16.6	16.5	16.1	15.4	15.3
Fe/Mn[a]	60.5	59.6	60.4	59.9	60.2	60.5	60.3	60.0	59.9	61.2	67.3	67.1
2σ	0.45	0.42	0.39	0.31	0.23	0.45	0.28	0.20	0.22	0.21	0.28	0.44
Fe/Mn[b]	60.1	59.7	60.5	59.7	60.2	60.1	61.7	62.0	62.0	61.7	68.6	66.2

Location	Caiyuan, Liaoning						Xiaogushan(Yitong), Jilin			Zhouba, Hebei			
Age	(36.3–39.3 Ma; Wang et al., 2007)						(10.4 Ma; Liu et al., 1992b)			(22.8 Ma; Liu et al., 1992b)			
Sample	WF1-1	WF1-2	WF2-1	WF2-2	WF2-4	WF2-7	YT-01	YT-02	YT-53	ZB-02	ZB-10	ZB-12	ZB-15
SiO_2	43.3	44.3	44.7	45.1	43.6	44.7	50.5	50.1	44.8	45.3	48.7	49.5	48.8
TiO_2	2.00	2.06	2.44	2.45	2.49	2.49	2.00	1.95	2.25	2.66	1.91	1.91	1.90

Table 1 (*continued*)

Location	Caiyuan, Liaoning						Xiaogushan(Yitong), Jilin			Zhouba, Hebei			
Age	(36.3–39.3 Ma; Wang et al., 2007)						(10.4 Ma; Liu et al., 1992b)			(22.8 Ma; Liu et al., 1992b)			
Sample	WF1-1	WF1-2	WF2-1	WF2-2	WF2-4	WF2-7	YT-01	YT-02	YT-53	ZB-02	ZB-10	ZB-12	ZB-15
Al_2O_3	12.5	12.9	12.1	12.3	12.0	12.2	15.5	15.5	14.3	14.2	14.4	14.4	14.5
Fe_2O_{3total}	11.9	12.1	12.4	12.5	12.3	12.5	11.3	11.3	11.4	13.5	11.3	11.4	11.2
MnO	0.16	0.17	0.15	0.14	0.15	0.15	0.14	0.14	0.16	0.16	0.14	0.14	0.13
MgO	8.13	8.64	10.2	10.1	9.98	10.1	7.87	7.72	10.3	8.04	8.81	8.00	7.66
CaO	12.8	12.7	11.9	11.8	11.9	12.3	7.25	7.61	8.52	8.72	7.78	8.05	8.10
Na_2O	1.74	1.91	1.88	1.86	1.92	1.88	3.96	3.76	2.92	2.86	2.68	2.80	2.86
K_2O	1.36	1.31	1.13	1.10	1.11	1.09	2.12	1.85	2.56	1.95	1.07	1.06	1.17
P_2O_5	0.42	0.44	0.29	0.28	0.29	0.29	0.59	0.60	0.63	0.80	0.33	0.33	0.36
LOI	5.52	3.12	2.85	2.38	3.78	1.81	0.55	1.46	1.87	1.70	3.12	2.52	2.89
Total	99.8	99.6	100.0	100	99.5	99.5	102	102	99.6	99.9	100	100	99.5
Mg#	57.8	58.8	62.2	61.8	61.8	61.7	58.1	57.7	64.4	54.3	60.9	58.5	57.7
Be	1.08	1.01	0.85	0.89	0.81	0.81	1.97	1.86	2.22	2.16	1.13	1.17	1.28
Sc	35.0	37.5	36.3	39.2	37.5	37.5	15.8	16.5	22.5	20.7	21.6	19.6	20.0
V	327	338	334	357	346	344	135	139	203	208	172	169	178
Cr	311	331	486	484	447	470	188	188	307	157	187	176	194
Co	47.0	47.7	53.6	56.8	53.3	54.4	41.2	39.4	51.9	56.0	50.4	45.8	47.1
Ni	97.9	100	154	157	139	148	90.3	78.1	243	157	158	143	149
Cu	80.3	84.5	71.0	71.3	72.1	70.9	23.4	21.1	47.4	71.0	56.1	55.3	50.3
Zn	87.6	102	78.8	82.0	82.5	81.0	125	125	86.5	146	107	104	103
Ga	18.0	18.7	16.5	17.5	17.1	16.8	23.9	23.3	20.2	23.7	19.9	19.9	20.4
Rb	25.3	20.4	15.7	16.2	15.4	15.1	22.0	23.3	26.5	32.0	17.0	17.7	19.2
Sr	916	932	611	649	641	616	781	750	816	812	368	389	436
Y	21.8	24.4	21.4	21.5	20.3	19.4	20.2	20.9	22.6	23.0	14.0	17.5	17.4
Zr	227	235	172	181	181	176	198	184	207	241	121	128	135
Nb	39.5	40.8	24.4	25.1	25.6	25.7	34.9	33.1	54.7	63.3	24.9	23.5	25.9
Cs	2.11	8.30	1.15	0.84	0.57	1.48	0.24	0.40	0.36	0.28	0.077	0.10	0.12
Ba	507	453	327	297	333	298	313	297	358	505	230	236	244
La	36.9	36.6	20.7	21.9	21.8	20.8	29.2	30.7	36.3	40.8	16.4	15.8	16.9
Ce	80.4	80.9	48.7	51.4	51.4	49.2	57.6	59.6	68.4	85.1	37.1	32.7	35.0
Pr	10.5	10.7	6.82	7.16	7.21	6.82	7.03	7.24	7.83	10.1	4.54	4.13	4.42
Nd	44.6	45.4	30.8	32.5	32.6	31.1	30.2	30.5	31.4	40.1	18.9	18.1	18.9
Sm	8.46	8.83	6.82	7.10	7.18	6.94	6.87	6.90	6.29	8.36	4.55	4.31	4.39
Eu	2.53	2.59	2.03	2.15	2.17	2.10	2.27	2.29	2.09	2.64	1.54	1.49	1.59
Gd	6.90	7.03	5.71	6.05	6.07	5.81	6.39	6.52	5.88	7.31	4.32	4.25	4.43
Tb	0.89	0.93	0.79	0.83	0.83	0.82	0.89	0.90	0.84	1.13	0.69	0.64	0.65
Dy	4.59	4.74	4.16	4.39	4.42	4.26	4.40	4.57	4.58	5.73	3.64	3.50	3.64
Ho	0.82	0.84	0.74	0.77	0.78	0.75	0.73	0.76	0.82	0.97	0.70	0.64	0.63
Er	2.08	2.07	1.79	1.90	1.92	1.87	1.80	1.87	2.13	2.19	1.59	1.63	1.61
Tm	0.27	0.27	0.23	0.24	0.24	0.23	0.24	0.25	0.31	0.25	0.20	0.22	0.22
Yb	1.64	1.65	1.37	1.46	1.46	1.39	1.32	1.42	1.72	1.42	1.17	1.25	1.19
Lu	0.23	0.23	0.19	0.20	0.21	0.20	0.19	0.20	0.25	0.18	0.16	0.18	0.17
Hf	5.10	5.24	4.28	4.58	4.53	4.36	4.31	4.02	4.39	5.47	3.10	2.96	3.07
Ta	2.36	2.40	1.56	1.61	1.66	1.59	2.44	2.27	3.73	4.29	1.67	1.55	1.70
Pb	6.15	11.0	4.28	4.32	3.72	3.66	5.10	4.72	4.96	3.87	2.74	8.84	12.2
Th	4.21	3.77	2.16	2.41	2.29	2.15	3.36	3.16	4.64	4.36	2.07	1.92	2.00
U	1.13	1.06	0.62	0.64	0.63	0.60	1.07	1.01	1.53	1.58	0.59	0.54	0.52
Zr/Nb	5.75	5.77	7.05	7.24	7.07	6.84	5.69	5.56	3.79	3.80	4.87	5.43	5.21
Nb/Ta	16.8	17.0	15.6	15.6	15.5	16.2	14.3	14.5	14.7	14.8	14.9	15.1	15.2
Fe/Mn[a]	59.0	59.0	66.7	68.6	66.6	66.4	66.6	69.3	62.0	76.8	72.5	73.6	76.4
2σ	0.28	0.28	0.31	0.39	0.24	0.34	0.21	0.22	0.19	0.32	0.30	0.29	0.29
Fe/Mn[b]	66.9	64.3	74.7	80.5	74.3	75.5	73.1	72.9	64.1	76.4	73.0	73.2	77.9

Location	Daxizhuang, Shandong				Qixia, Shandong					
Age	(73.0 Ma; Yan et al., 2005)				(8.1-6.2 Ma; Liu et al., 1992b)					
Sample	DX-6	DX-9	DX-17	DX-23	QX-72	QX-73	QX-77	QX-92	QX-99	QX-103
SiO_2	44.3	44.1	44.4	44.4	39.9	39.7	39.8	39.9	39.7	39.7
TiO_2	2.48	2.55	2.50	2.52	2.52	2.53	2.50	2.51	2.51	2.51
Al_2O_3	14.1	14.1	14.1	14.0	11.1	11.2	11.4	11.4	11.2	11.3
Fe_2O_{3total}	13.3	13.5	13.2	13.3	14.9	14.7	14.7	14.7	14.6	14.6

(*continued on next page*)

Table 1 (*continued*)

Location	Daxizhuang, Shandong				Qixia, Shandong					
Age	(73.0 Ma; Yan et al., 2005)				(8.1-6.2 Ma; Liu et al., 1992b)					
Sample	DX-6	DX-9	DX-17	DX-23	QX-72	QX-73	QX-77	QX-92	QX-99	QX-103
MnO	0.16	0.16	0.16	0.16	0.21	0.21	0.21	0.21	0.21	0.21
MgO	9.45	9.37	9.31	9.14	10.8	10.7	10.3	10.3	9.75	10.3
CaO	8.71	8.93	8.72	9.05	11.5	11.3	11.6	11.4	13.2	11.5
Na_2O	4.04	4.18	4.15	3.98	3.91	3.76	3.90	4.06	3.19	3.75
K_2O	1.78	1.20	1.78	1.40	2.26	2.18	2.26	2.33	1.64	2.20
P_2O_5	0.64	0.66	0.64	0.65	0.76	0.80	0.92	0.85	0.91	0.82
LOI	1.00	1.09	0.98	1.31	1.79	2.59	2.03	2.02	2.71	2.66
Total	99.9	99.8	100.0	99.9	99.6	99.6	99.6	99.6	99.6	99.6
Mg#	58.6	58.2	58.5	57.9	59.3	59.3	58.3	58.3	57.2	58.6
Be	2.27	2.39	2.24	2.32	4.41	4.28	4.51	4.39	4.49	4.37
Sc	21.1	20.7	21.7	20.9	13.2	13.2	12.9	13.3	12.5	13.5
V	214	219	216	217	175	175	174	177	178	172
Cr	165	161	165	159	201	247	216	190	199	184
Co	50.8	51.7	51.0	51.2	50.5	50.4	49.7	50.4	50.3	48.7
Ni	190	188	189	183	153	151	142	147	146	143
Cu	54.6	52.9	55.8	52.9	41.0	41.4	40.4	41.4	39.7	40.0
Zn	101	103	101	100	159	159	159	162	162	156
Ga	20.5	21.4	21.1	21.1	25.7	26.3	26.7	26.7	25.6	26.3
Rb	25.1	24.8	25.6	29.1	26.3	26.6	25.1	26.4	21.0	25.8
Sr	717	773	724	833	1173	1309	1574	1246	3075	1425
Y	29.5	28.0	29.8	27.6	30.0	29.6	30.2	30.5	30.4	30.3
Zr	258	266	260	263	396	393	395	397	396	394
Nb	61.2	63.3	62.9	62.8	119	120	123	123	121	121
Cs	0.37	0.54	0.38	0.45	0.42	0.63	0.44	0.47	0.40	0.44
Ba	406	411	416	418	277	399	362	202	564	355
La	38.6	39.8	39.6	39.5	90.9	89.5	92.8	94.1	92.8	93.1
Ce	75.4	78.0	77.9	77.8	167	166	169	172	172	171
Pr	8.98	9.36	9.27	9.29	19.4	19.2	19.5	19.7	19.7	19.8
Nd	36.2	37.7	37.5	37.6	75.7	75.0	75.6	76.7	75.9	76.4
Sm	7.45	7.79	7.70	7.80	13.6	13.7	13.9	14.0	13.8	13.9
Eu	2.33	2.43	2.39	2.41	4.27	4.23	4.30	4.24	4.39	4.29
Gd	6.77	6.97	6.90	6.96	11.7	11.5	11.7	11.8	11.9	11.8
Tb	0.98	1.01	1.02	1.01	1.53	1.49	1.52	1.53	1.54	1.53
Dy	5.35	5.52	5.56	5.55	7.07	7.04	7.04	7.12	7.11	7.08
Ho	0.99	1.01	1.00	1.01	1.10	1.06	1.13	1.12	1.11	1.11
Er	2.49	2.57	2.58	2.60	2.39	2.39	2.44	2.47	2.48	2.44
Tm	0.32	0.33	0.34	0.33	0.29	0.29	0.29	0.30	0.29	0.29
Yb	1.99	1.99	2.04	2.04	1.48	1.45	1.45	1.46	1.43	1.43
Lu	0.25	0.27	0.27	0.27	0.18	0.18	0.18	0.18	0.18	0.18
Hf	5.59	5.77	5.78	5.79	8.02	8.07	8.05	8.03	8.03	8.00
Ta	3.99	4.18	4.18	4.14	8.54	8.67	8.78	8.73	8.60	8.69
Pb	5.13	4.91	5.32	5.20	8.47	8.57	8.64	8.89	10.0	8.73
Th	5.04	5.13	5.24	5.19	12.3	12.2	12.6	12.7	12.3	12.7
U	1.44	1.46	1.50	1.48	3.70	3.38	4.02	4.08	3.57	3.64
Zr/Nb	4.21	4.20	4.14	4.18	3.32	3.28	3.23	3.23	3.28	3.25
Nb/Ta	15.4	15.1	15.0	15.2	14.0	13.8	14.0	14.1	14.1	13.9
Fe/Mn[a]	61.9	62.6	61.9	62.1	60.7	61.0	60.8	60.8	61.1	60.0
2σ	0.27	0.26	0.28	0.29	0.19	0.21	0.17	0.22	0.18	0.22
Fe/Mn[b]	75.2	76.0	74.7	74.9	63.9	63.1	63.3	63.2	62.8	62.8
Location	Guizishan(Liuhe), Jiangsu			Fangshan (Liuhe), Jiangsu			Jiashan, Anhui			
Age				(8.6 Ma; Liu et al., 1992b)			(1.41 Ma; Liu et al., 1992b)			
Sample	GZS00-01	GZS00-02	GZS00-08	FS00-02	FS00-55	FS00-59	LS99-01	LS99-03	NS99-06	NS99-16
SiO_2	43.7	43.6	45.6	47.0	47.4	47.6	45.6	46.7	43.5	43.7
TiO_2	2.20	2.22	2.17	2.14	2.16	2.14	2.78	2.78	2.23	2.22
Al_2O_3	12.3	12.3	12.8	13.9	14.0	14.0	13.2	12.8	13.8	13.8
Fe_2O_{3total}	13.2	13.0	12.5	11.5	11.4	11.3	13.4	12.2	13.3	13.2
MnO	0.18	0.18	0.17	0.14	0.14	0.14	0.17	0.16	0.18	0.17
MgO	10.5	10.4	10.6	9.63	9.50	10.2	9.11	9.27	9.06	9.10
CaO	9.62	9.74	9.16	7.45	7.25	7.21	8.83	8.61	8.00	7.85

Table 1 (*continued*)

Location	Guizishan(Liuhe), Jiangsu			Fangshan (Liuhe), Jiangsu (8.6 Ma; Liu et al., 1992b)			Jiashan, Anhui (1.41 Ma; Liu et al., 1992b)			
Age										
Sample	GZS00-01	GZS00-02	GZS00-08	FS00-02	FS00-55	FS00-59	LS99-01	LS99-03	NS99-06	NS99-16
Na_2O	4.10	4.14	3.12	3.53	3.39	3.22	2.96	2.20	4.37	5.39
K_2O	1.54	1.46	1.76	2.02	1.91	2.37	1.93	1.82	1.87	3.18
P_2O_5	0.95	0.95	0.68	0.52	0.51	0.51	0.70	0.73	1.22	1.21
LOI	1.30	1.53	1.10	1.85	1.96	0.92	1.53	3.03	2.50	0.32
Total	99.6	99.5	99.6	99.6	99.6	99.6	100	100	100.0	100
Mg#	61.4	61.6	62.8	62.6	62.6	64.2	57.6	60.2	57.7	58.1
Be	2.38	2.45	1.99	1.90	1.99	1.94	2.22	2.37	3.06	3.03
Sc	18.5	13.8	20.2	16.3	15.9	16.0	19.4	18.0	10.8	11.8
V	178	169	188	143	144	146	213	183	139	144
Cr	274	265	293	341	319	348	226	281	274	251
Co	53.4	53.5	53.5	48.8	48.3	48.3	99.9	75.1	72.4	101
Ni	251	258	252	296	289	289	203	227	242	226
Cu	58.8	56.5	45.6	57.1	54.8	54.2	73.3	62.4	38.7	38.8
Zn	129	126	116	104	103	104	136	127	146	148
Ga	21.2	20.5	21.0	20.6	20.7	20.9	23.3	21.3	24.7	24.4
Rb	33.7	30.0	35.3	36.5	42.1	42.6	24.4	22.9	66.1	55.5
Sr	948	902	812	722	725	682	781	836	1381	1209
Y	26.2	24.8	23.7	20.5	20.4	19.9	24.5	25.2	23.1	22.4
Zr	211	210	183	186	185	180	221	218	256	244
Nb	71.3	69.1	56.4	50.2	50.0	48.9	52.8	51.8	94.8	90.5
Cs	0.55	0.68	0.46	0.62	0.85	0.66	0.26	0.15	0.90	0.80
Ba	454	436	524	408	414	406	390	347	526	522
La	51.6	49.1	37.4	27.8	27.7	27.5	34.4	37.9	62.7	57.9
Ce	94.1	90.0	69.1	53.6	53.0	52.6	66.0	70.8	111	104
Pr	10.9	10.4	8.17	6.26	6.25	6.19	7.97	8.39	12.7	12.0
Nd	43.7	41.8	33.5	25.2	25.4	25.1	32.9	35.1	50.0	47.4
Sm	8.90	8.42	7.01	5.44	5.50	5.56	7.05	7.56	9.57	9.23
Eu	2.96	2.79	2.39	1.90	1.88	1.88	2.46	3.11	3.20	3.07
Gd	8.31	7.87	6.72	5.42	5.38	5.39	6.99	7.50	8.55	8.24
Tb	1.12	1.08	0.96	0.78	0.78	0.76	0.99	1.06	1.12	1.08
Dy	5.80	5.45	5.12	4.25	4.20	4.16	5.22	5.42	5.31	5.21
Ho	0.96	0.91	0.86	0.75	0.74	0.72	0.86	0.91	0.82	0.81
Er	2.30	2.20	2.12	1.84	1.82	1.82	2.22	2.26	1.84	1.79
Tm	0.29	0.27	0.27	0.26	0.25	0.24	0.28	0.28	0.21	0.21
Yb	1.55	1.53	1.52	1.42	1.42	1.35	1.55	1.56	1.10	1.06
Lu	0.21	0.19	0.21	0.19	0.19	0.19	0.21	0.21	0.13	0.13
Hf	4.62	4.53	4.10	4.22	4.18	4.10	4.86	4.96	5.38	5.20
Ta	4.57	4.33	3.69	3.30	3.26	3.20	3.73	3.52	6.30	6.06
Pb	5.86	6.45	4.23	3.93	4.17	4.24	4.50	4.70	5.91	4.92
Th	7.36	6.51	5.28	4.00	4.02	3.93	4.03	4.58	8.34	7.83
U	1.87	1.80	1.41	1.18	1.19	1.17	1.22	0.95	2.34	2.30
Zr/Nb	2.96	3.03	3.25	3.70	3.70	3.69	4.18	4.21	2.70	2.70
Nb/Ta	15.6	16.0	15.3	15.2	15.3	15.3	14.2	14.7	15.0	14.9
Fe/Mn[a]	64.0	63.1	64.9	69.8	71.0	70.5	69.9	68.9	68.0	68.3
2σ	0.13	0.14	0.21	0.19	0.22	0.17	0.27	0.26	0.25	0.28
Fe/Mn[b]	66.4	65.2	66.5	74.1	73.3	73.1	71.2	69.1	66.5	69.9

[a] Measured by ICP-MS.
[b] Calculated according to the oxides determined by XRF.

in Nb and Ta) (Fig. 4d). The relatively high Pb of some <110 Ma basalts may have inherited from recycled crust as discussed in Section 5. Their Nb and Ta contents (average values = 60.1 and 4.01 ppm, respectively) are higher than those of >110 Ma basalts (average values = 10.8 and 0.54 ppm, respectively) by a factor of 6–8. The low Zr/Nb ratios (2.7–8.1) of the <110 Ma basalts are similar to those observed in OIBs (2.36–9.88; Pfänder et al., 2007). Except for two high-MgO Luanshishanzi basalts, Nb, Ta and Y correlate positively with MgO (Fig. 5a–c). The relatively high MgO contents of the Luanshishanzi basalts may have resulted from olivine accumulation, as suggested by their high Cr and Ni contents (Table 1).

As a whole, Nb/Ta and Fe/Mn ratios of the basalts change with age (Fig. 6a). The >110 Ma basalts are characterized by superchondritic Nb/Ta ratios (20.1 ± 0.3 (2σ, $n = 25$)) and Fe/Mn ratios (60.0 ± 1.1 (2σ, $n = 25$)) that lie between the average Fe/Mn ratios of MORB (56.2,

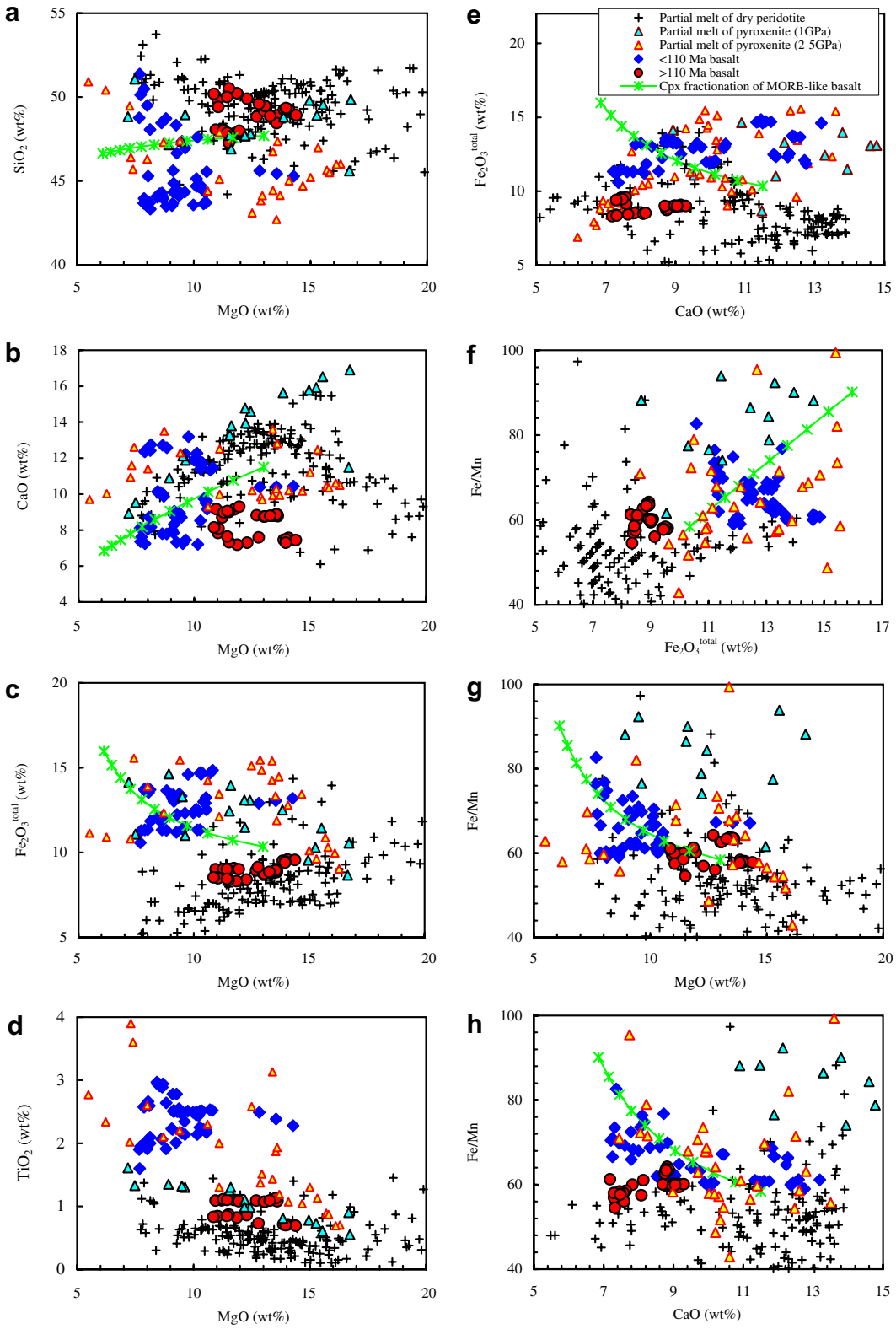

Fig. 3. Plots of MgO–SiO_2, –CaO,—total Fe_2O_3, –TiO_2 and –Fe/Mn and total Fe_2O_3–CaO and –Fe/Mn for basalts from the East China. Basaltic melts of pyroxenite at 1 GPa (Kogiso and Hirschmann, 2001) and 2–5 GPa (Hirschmann et al., 2003; Kogiso et al., 2003; Pertermann and Hirschmann, 2003a,b; Keshav et al., 2004; Kogiso and Hirschmann, 2006), and dry peridotite at 0.1–7 GPa (Hirose and Kushiro, 1993; Baker and Stolper, 1994; Walter, 1998; Falloon and Danyushevsky, 2000; Xu et al., 2006; Schwab and Johnston, 2001; Wasylenki et al., 2003; Laporte et al., 2004) are shown for comparison. Cpx crystal fractionation of MORB-like basalt was simply calculated according to batch crystallization model. Because olivine fractionation would decrease Fe/Mn ratio of the melt, thus only cpx was taken into account to evaluate the contribution of crystal fractionation to the high Fe/Mn ratios of <110 Ma basalts. Parameters used in calculations are listed in Table 2. Each cross on the line represents 10% increment of crystallization degree.

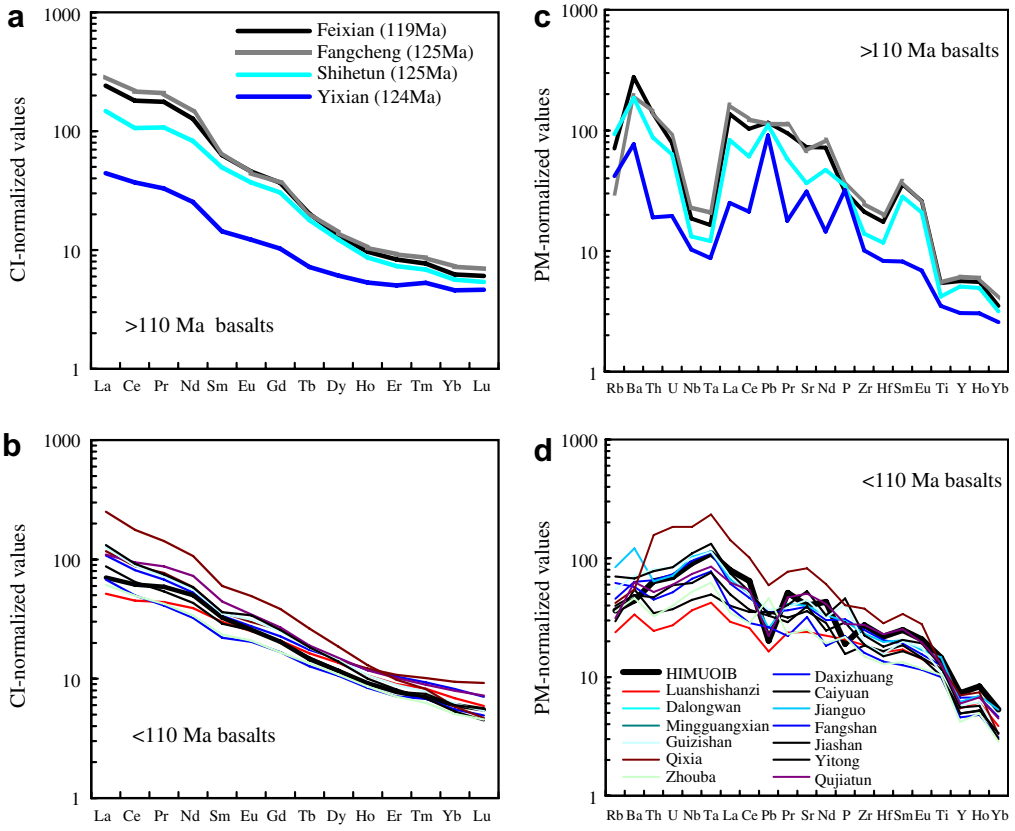

Fig. 4. CI-normalized REE patterns and PM-normalized trace element patterns for the Mesozoic and Cenozoic basalts. Chondrite (CI) values from Taylor and McLennan (1985), Primitive Mantle (PM) values from McDonough and Sun (1995). Each line represents a basalt locality. HIMU OIB from Rurutu from Chauvel et al. (1997).

$n = 678$, RidgePetDB) and continental flood basalts (63.2, $n = 5108$, GEOROC). In contrast, the <110 Ma basalts have higher Fe/Mn (64.7 ± 1.5 (2σ, $n = 45$)) and lower Nb/Ta (15.4 ± 0.3 (2σ, $n = 45$)) ratios. Fe/Mn ratios of the <110 Ma basalts cluster within the range of 59–77 regardless of their total Fe_2O_3, MgO and CaO contents (Fig. 3f–h). In the MnO–Fe/Mn diagram, the <110 Ma basalts overlap with the Hawaiian and Iceland OIBs (Fig. 1d).

Finally, we note that Fe/Mn ratios in the <110 Ma basalts correlate negatively with HREE (e.g., Yb, correlation coefficient = −0.65; Fig. 6b) and Y. Except for the Caiyuan basalts, Yb correlates positively with Sc (Fig. 6c). The Caiyuan basalts show specific Sc enrichment relative to Yb. In contrast, Fe/Mn ratios in the >110 Ma basalts correlate positively with CaO, Yb and Y (correlation coefficient = 0.65, 0.47 and 0.54, respectively), but not with MgO (Figs. 3g and h and 6b). Yb correlates negatively with Sc (Fig. 6c).

5. DISCUSSION

5.1. Contrasting Nb/Ta ratios of the Cenozoic and Mesozoic basalts: role of rutile-bearing eclogite

The significance of the different Nb/Ta ratios between the <110 and >110 Ma basalts will be discussed first. We will show that the contrasting Nb/Ta ratios reflect different mantle sources. However, before doing so, we rule out the possibility that the Nb/Ta differences are artifacts of magmatic differentiation in the form of crystal fractionation of Fe–Ti-oxides and crustal contamination as follows. Average bulk continental crust is characterized by low Nb/Ta ratio (11.4), and Nb (Ta) depletions (Rudnick and Gao, 2003). Nb (8 ppm) and Ta (0.7 ppm) contents of the bulk continental crust (Rudnick and Gao, 2003) are remarkably lower than that of the <110 Ma basalts (Table 1). Simple mixing calculations suggest that, for initial melt with Nb/Ta = 17.5 and Nb = 23 ppm (minimum of the <110 Ma basalts), >40% continental crust is needed to match the Nb/Ta ratios of <110 Ma basalts by crustal contamination. Such high crustal contamination would not only result in low Nb/Ta ratios, but also yield Nb and Ta depletions relative to La in the trace element patterns, which are not observed in the <110 Ma basalts (Fig. 4d). Both Nb and Ta are moderately compatible in Ti–Fe-oxides in equilibrium with basaltic melts ($D_{Nb} = 0.6$-1.9 and $D_{Ta} = 1.2$-2.7), and Ta is more compatible then Nb ($D_{Nb}/D_{Ta} = 0.50 - 0.75$) (Klemme et al., 2006). Crystal fractionation of Fe–Ti-oxides would lightly increase Nb/Ta ratios of the melts, which precludes contributions from crystal fractionation of Ti–Fe-oxides for the low Nb/Ta ratios of the <110 Ma basalts. The Nb/Ta ratios of the >110 Ma basalts are too high to be produced by single crystal fractionation of Fe–Ti-oxides. Given a Nb/Ta ratio of 17.5

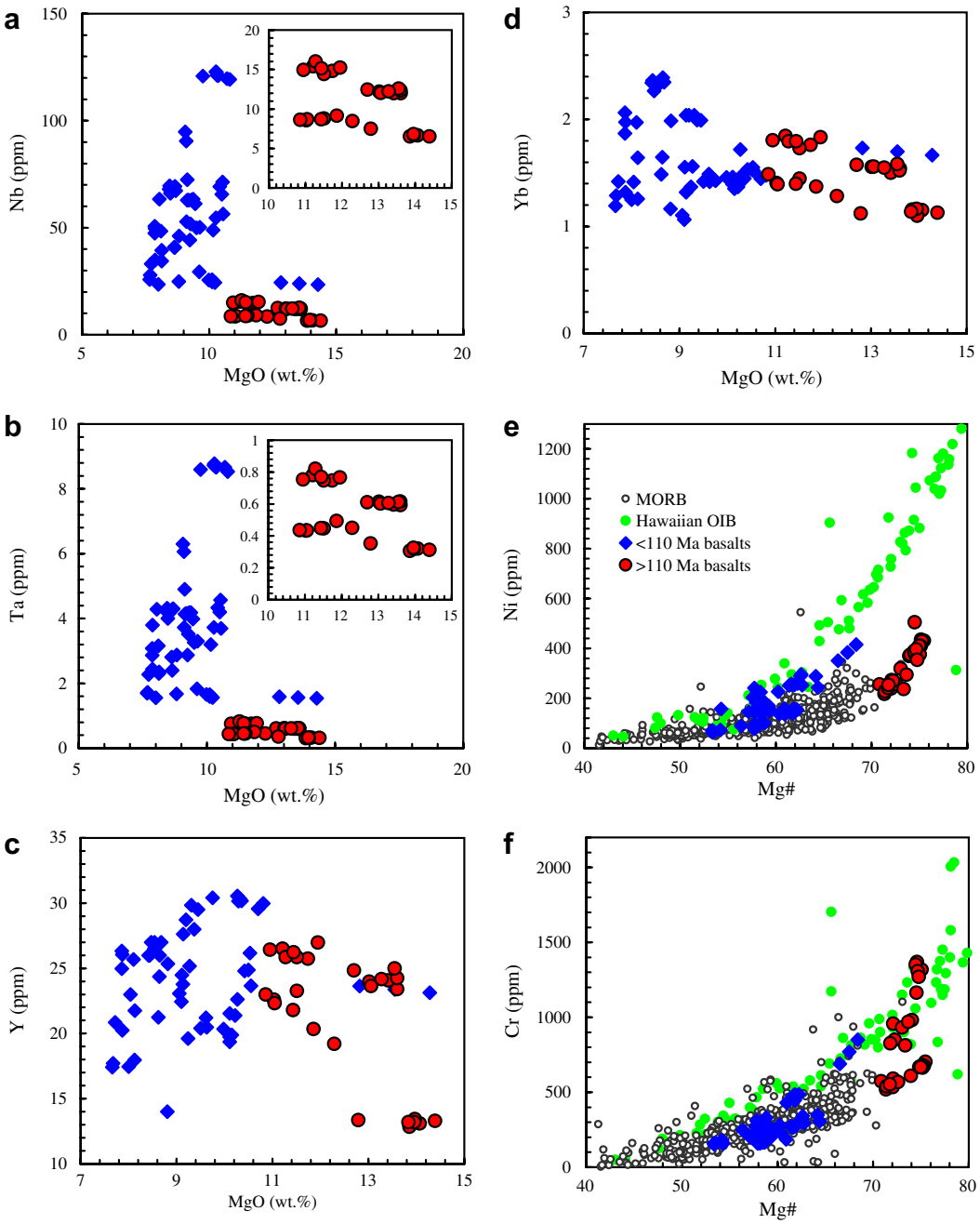

Fig. 5. Plots of MgO–Nb, –Ta, –Y and –Yb and Mg#–Ni and –Cr for the basalts. Middle Ocean Ridge Basalts (MORB) ($n = 809$) (http://www.ldeo.columbia.edu/RidgePetDB) and Hawaiian OIB (Gaffney et al., 2004; Mukhopadhyay et al., 2003; Norman and Garcia, 1999) are also shown for comparison.

for the initial melt, unreasonably high crystal fractionation (10-30%) of Fe–Ti-oxides were needed to produce the high Nb/Ta ratios of the >110 Ma basalts (Fig. 6e). Therefore, even though crystal fractionation of Fe–Ti-oxides may have played a role in elevating the Nb/Ta ratios of the >110 Ma basalts, high Nb/Ta initial melts are required. On the other hand, although the >110 Ma basalts contain 2–15% of ol, cpx and opx phenocrysts, <15% of phenocrysts would contribute <1% to Nb/Ta ratio of the resultant melt due to the high incompatibility of Nb and Ta in ol, cpx and opx (Dunn and Sen, 1994; Hauri et al., 1994). Furthermore, addition of these phenocrysts would reduce the Nb/Ta ratio due to $D_{Nb} < D_{Ta}$ for ol, cpx and opx (Dunn and Sen, 1994; Hauri et al., 1994), which is inconsistent with the high Nb/Ta ratios of the >110 Ma basalts. For these reasons, we explore source effects below.

The negative correlations between MgO and Nb and Ta for the >110 Ma basalts (Fig. 5a and b) indicate that both Nb and Ta are highly incompatible during mantle melting. Therefore, their low Nb and Ta contents and high Nb/Ta

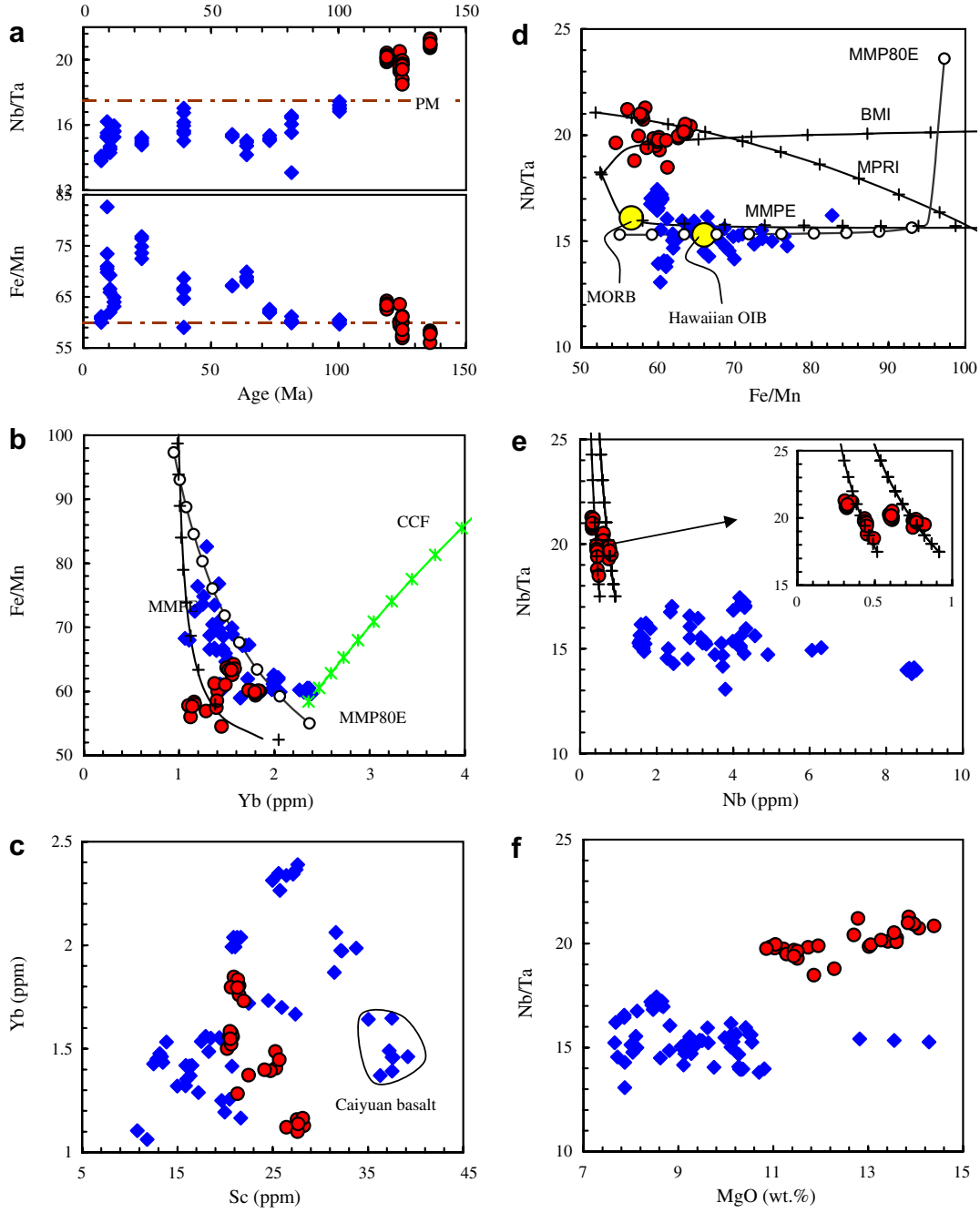

Fig. 6. (a) Variations of Nb/Ta and Fe/Mn ratios with age, (b and c) Plots of Yb vs. Sc and Fe/Mn ratio, (d–f) Plots of Nb/Ta ratio vs. Nb, MgO and Fe/Mn ratio. MPRI, BMI and MMPE in (b) and (d) are partial melts of mixtures of peridotite + secondary pyroxenite formed by peridotite-melt reaction by infiltration (MPRI) and injection (BMI), and mechanical mixture of peridotite + eclogite (MMPE). Silicic melt was assumed to be produced by 10% partial melting of recycled lower continental crust (Table 2). Melting degrees are 1%, 10% and 10% for MPRI, BMI and MMPE, respectively. Each plus on the lines represents a 10% increment of pyroxenite. MMP80E are partial melts of 20% peridotite + 80% eclogite. Each circle on the line represents an increment of 10% partial melting. CCF = Cpx crystal fractionation of MORB-like primary basalt, which was calculated according to equilibrium crystal fractionation. FTOCF = Crystal fractionation of Fe–Ti-oxides (each plus represents a 10% increment of Fe–Ti-oxide crystallization, partition coefficients from Klemme et al. (2006)). The other symbols as in Fig. 3. MORB is average of Middle Ocean Ridge Basalts ($n = 809$; http://www.ldeo.columbia.edu/RidgePetDB). Fe/Mn ratio from Humayun et al. (2004) and Nb/Ta ratio from Pfänder et al. (2007) for Hawaiian OIB.

ratios suggest low-Nb and -Ta mantle sources with high Nb/Ta ratios. Negative correlation between Nb/Ta ratio and MgO is expected for partial melting of ol + cpx + opx assemblage because D_{Nb}/D_{Ta} is <1 for ol, cpx and opx (Dunn and Sen, 1994; Hauri et al., 1994). Although both Nb and Ta are incompatible in amphibole, D_{Nb}/D_{Ta} is >1 for low-Mg# amphiboles (Tiepolo et al., 2000), and $D_{Nb,\,Ta}^{amphibole}$ is significantly higher than $D_{Nb,\,Ta}^{ol,\,cpx\ and\ opx}$

Table 2
Partition coefficients and chemical compositions of different end members used in the calculations

Element	SiO_2	Fe_2O_3[a]	MnO	MgO	CaO	Rb	Ba	Th	U	Nb	Ta	La	Ce	Pb	Pr	Sr	Nd	Zr	Hf	Sm	Eu	Y	Ho	Yb
	Contents (unit = wt%)					*Contents (unit = ppm)*																		
RCC	52.2	12.5	0.197	5.44	8.30	30.7	194	3.11	0.45	7.07	0.45	13.0	33.5	7.52	3.66	192	15.7	76.0	2.80	3.85	1.18	27.9	0.98	2.61
MP						0.040	1.20	0.014	0.005	0.112	0.006	0.234	0.772	0.023	0.131	12.9	0.74	7.94	0.199	0.30	0.107	4.07	0.122	0.401
MORB	47.7	10.4	0.16	13.0	11.5																			
	Partition coefficients					*Partition coefficients between minerals and mafic melt*																		
cpx	1.02	0.65	1.00	2.14	1.68	0.0018	0.006	0.0032	0.0041	0.005	0.011	0.027	0.055	0.042	0.062	0.067	0.122	0.10	0.22	0.19	0.179	0.47	0.256	0.55
Garnet	0.79	1.36	3.00	2.73	0.88	0.0050	0.005	0.0008	0.0045	0.005	0.004	0.012	0.005	0.056	0.027	0.010	0.057	0.19	0.22	0.19	0.208	2.62	1.60	5.71
Ref.						P	P	P	P	P	P	P	P	P	T	P	P	P	P	P	P	P	T	P
opx	1.12	0.74	0.82	2.35	0.17	0.0006	0.001	0.0001	0.0001	0.010	0.020	0.0003	0.0005	0.001	0.0013	0.0048	0.002	0.0068	0.02	0.01	0.01	0.013	0.02	0.026
Ref.						M	W	M	M	G	G	K	K	K	M	M	K	M	K	M	M	M	M	M
ol	0.83	1.17	0.87	3.47	0.03	0.00018	0.00000	0.00000	0.00001	0.00017	0.00002	0.0130	0.00006	0.00006	0.000069	0.000026	0.000039	0.00015	0.0045	0.0037	0.00044	0.00056	0.0038	0.0047
Ref.	A1	A1	A1	A1	A1	M	B	B	B	Z	Z	Z	Z	Z	B	B	B	Z	Z	Z	Z	Z	Z	B
						Partition coefficients between minerals and felsic melt																		
Cpx						0.060	0.070	0.070	0.050	0.010	0.070	0.120	0.200	0.021	0.320	0.050	0.48	0.08	0.10	0.86	1.04	1.63	1.67	1.77
Garnet						0.001	0.000	0.030	0.080	0.004	0.025	0.003	0.014	0.044	0.052	0.002	0.17	0.92	0.51	0.96	1.80	9.30	10.2	17.2
Ref.						X	X	X	X	X	X	BF	BF	P	BF	X	BF	X	X	BF	BF	BF	BF	BF
Rutile						0.0076	0.0137	0.054		144	177	0.0055	0.087	0.0154		0.036	0.277	4.24	5.32	0.016	0.0004	0.007	0.000	0.0093
Ref.						F	F	F		A2	A2	F	F	F		F	F	F	F	F	F	F	F	F

RCC = Recycled continental crust, represented by mixture of 80% Archean mafic granulite +20% Archean metasediment from the North China Craton (Liu et al., 2004); MP = Mantle peridotite represented by depleted mantle (Salters and Stracke, 2004); MORB = Average of MORB with MgO = 11–15 wt% (http://www.ldeo.columbia.edu/RidgePetDB); A1 = Calculated according to experiments (data sources are the same as in Fig. 1); A2 = Calculated for felsic melt (melting degree = ~10%) in this works; B = (Beattie, 1993); BF = (Barth et al., 2002); F = (Foley et al., 2000); G = (Green et al., 1993); K = (Keleman and Dunn, 1992); M = (McKenzie and O'Nions, 1991); P = (Pertermann et al., 2004); T = (Tuff and Gibson, 2007); W = (Walker et al., 1992); X = (Xiong, 2006); Z = (Zanetti et al., 2004).

[a] Total Fe_2O_3.

(Dunn and Sen, 1994; Hauri et al., 1994). Therefore, the positive correlation between MgO and Nb/Ta ratio for the >110 Ma basalts (Fig. 6f) suggests amphibole-bearing mantle sources, which could be produced by melt–peridotite reaction (Rapp et al., 1999). The positive correlations between MgO and Nb and Ta for the <110 Ma basalts (Fig. 5a and b) indicate that both Nb and Ta are compatible during mantle melting. This points to the dominant role of Ti–Fe oxides (e.g., rutile and ilmenite). The constant Nb/Ta ratios, regardless of MgO contents, suggest that Nb/Ta ratios of the melts were budgeted by Nb- and Ta-rich Ti–Fe oxides (Fig. 6f).

At the same pressures, recycled mafic crustal rocks have lower melting points than peridotite (Yasuda et al., 1994; Hirschmann and Stolper, 1996; Hirschmann, 2000; Keshav et al., 2004) and thus melt preferentially to produce silicic melts and eclogitic residues (Yaxley and Green, 1998; Rapp et al., 1999; Yaxley, 2000; Rapp et al., 2003; Kessel et al., 2005a; Kessel et al., 2005b). Depending on the depth of melt generation, these melts/fluids must traverse part of the mantle while the complementary eclogitic residues would founder into the mantle due to their higher densities ($\rho = 3.30$–3.65 g/cm^3) compared to ambient peridotitic mantle ($\rho = 3.30$–3.50 g/cm^3) (Ringwood and Green, 1966; Herzberg et al., 1983; Anderson, 2005). Melt–peridotite interaction is thus inevitable even beneath ocean ridges (Niu, 2004). While some parts of the upper mantle represent solid residues of peridotite partial melting, it is likely that other parts represent the end-products of (1) metasomatic reactions between peridotitic mantle and eclogite-derived melts/fluids that have traversed the mantle or (2) mechanical mixing between mantle peridotite and foundered eclogitic residues. The compositions of these hybridized reservoirs are of interest here.

The question is how these sorts of mantle heterogeneities are manifested in terms of Nb and Ta systematics. In this context, it is worth noting that both natural eclogite samples (Rudnick et al., 2000; Zhang et al., 2000; Jacob, 2004; Xu et al., 2004; Xu et al., 2006) and experimental products of pyroxenite melting (Rapp and Watson, 1995; Kogiso et al., 1997; Rapp et al., 1999; Pertermann and Hirschmann, 2003a; Dasgupta et al., 2004) indicate that rutile is a common mineral phase. Since rutile fractionates Nb and Ta (Foley et al., 2000; Klemme et al., 2005; Xiong et al., 2005), distinct Nb and Ta systematics might be predicted for each of the mantle reservoirs predicted above as long as rutile was present during magma-genesis. Klemme et al. (2002) suggested that TiO_2 concentrations in the protoliths necessary for rutile saturation in melts are >1.6 wt%. However, mass balance calculations, based on the recent experiments (Barth et al., 2002; Pertermann et al., 2004; Schmidt et al., 2004; Xiong et al., 2005), suggest that rutile content in the residue (and thus bulk $D_{(Nb,Ta)}$) depends on not only the TiO_2 concentration of the protolith and partial melting degree (Fig. 7), but also on temperature and pressure conditions as suggested by experiments (Green and Pearson, 1986; Ryerson and Watson, 1987; Klemme et al., 2002; Xiong et al., 2005). This is consistent with the observations that some experimental melts possess higher Nb and Ta contents than the source rock, while others have lower Nb and Ta contents than the source rock (Rapp et al., 2003; Xiong et al., 2005). We modeled the proportion of TiO_2, and thus rutile, in eclogitic residues (Fig. 7). For partial melting of basaltic rock with $TiO_2 = 1.6$ wt% at 950–1200 °C and 1.5–2.5 GPa, rutile will not disappear from the residue until the melt fraction exceeds 80%.

Since rutile appears to be a residual phase, we can now explore the resulting Nb and Ta systematics on the eclogitic

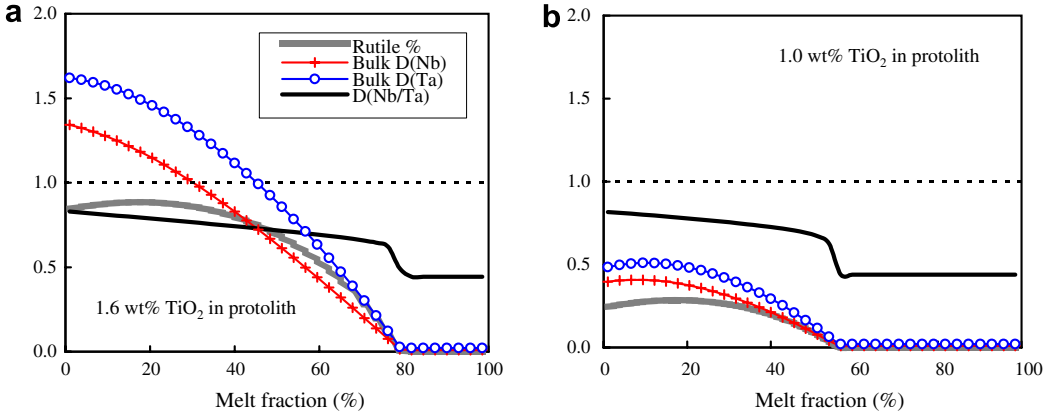

Fig. 7. Variations of rutile contents and bulk partition coefficients for Nb and Ta during melting of basaltic rocks. Mass balance calculations were conducted with two kinds of protoliths with $TiO_2 = 1.6$ wt% (a) and 1.0 wt% (b), and assuming eclogite (gar + cpx + rutile) as residue. A linear relationship between the melt fractions and chemical compositions (except for TiO_2) was constructed using the experimental results of Sen and Dunn (1994) and Xiong et al. (2005) to calculate major element compositions of partial melts. These experiments using basaltic lithologies as starting materials (Sen and Dunn, 1994; Xiong et al., 2005). The TiO_2 contents of melts saturated in rutile and $D_{(Nb,\,Ta)}^{rutile/melt}$ values were calculated with $TiO_2 = 0.374 \cdot \exp(0.589 \cdot FM)$, $D_{Nb}^{rutile/melt} = 259 \cdot \exp(-0.542 \cdot FM)$ and $D_{Ta}^{rutile/melt} = 274 \cdot \exp(-0.406 \cdot FM)$ ($FM = [Na + K + 2(Ca + Fe + Mg)]/Al1/Si$; Ryerson and Watson, 1987) based on the experiments of Schmidt et al. (2004) and Xiong et al. (2005). For gar and cpx, partition coefficients of Nb and Ta were assumed to be $D_{Nb}^{gar} = 0.010$, $D_{Ta}^{gar} = 0.014$, $D_{Nb}^{cpx} = 0.009$ and $D_{Ta}^{cpx} = 0.024$ (Barth et al., 2002; Pertermann et al., 2004); and partition coefficients of Ti were calculated with $D_{Ti}^{gar} = 0.0078 \cdot \exp(0.070 \cdot SiO_2)$ and $D_{Ti}^{cpx} = 0.0086 \cdot \exp(0.072 \cdot SiO_2)$ based on the experiments of Barth et al. (2002) and Pertermann et al. (2004).

melt and complementary eclogitic residue. Experimental studies demonstrate that rutile sequesters Nb and Ta ($D_{Nb,\ Ta}^{rutile/melt} \gg 1$) and at the same time fractionates Ta from Nb ($D_{Nb}/D_{Ta}^{rutile/melt} = 0.21 - 1.0$) (Green and Pearson, 1987; Ryerson and Watson, 1987; Wendlandt, 1990; Ayers and Watson, 1991; Brenan et al., 1994; Stalder et al., 1998; Foley et al., 2000; Schmidt et al., 2004; Klemme et al., 2005; Xiong et al., 2005). Furthermore, $D_{Nb,\ Ta}^{rutile/melt}$ values and D_{Nb}/D_{Ta} ratios depend on melt composition, without any significant correlation with rutile composition. Both $D_{Nb,\ Ta}^{rutile/melt}$ values and D_{Nb}/D_{Ta} ratios increase with increasing SiO_2 contents of the melts (Schmidt et al., 2004; Klemme et al., 2005; Xiong et al., 2005). Using these partition coefficients, bulk Nb and Ta partition coefficients for rutile-bearing eclogites with $TiO_2 = 1.6$ wt% are always >1 at melt fraction <30% (Fig. 7a). Finally, this means that small degree melts in equilibrium with rutile-bearing eclogites would have high Nb/Ta ratios but low Nb and Ta contents while the rutile-bearing eclogite residue would have low Nb/Ta ratios but high Nb and Ta contents, consistent with the low Nb/Ta ratios of rutiles from eclogites (Zack et al., 2002).

We now return to the two types of mantle reservoirs generated by the partial melting of recycled eclogites: (1) hybridized mantle formed by reaction between small-degree partial melts of rutile-bearing eclogite and peridotitic mantle, and (2) hybridized mantle formed by mechanical mixing of foundered eclogitic residues and peridotitic mantle (Fig. 6d). Assuming that rutile persists as a magmatic phase in the eclogitic residues, the following would be predicted. Peridotitic mantle metasomatized by small degree melts of rutile-bearing eclogite would be characterized by high Nb/Ta ratios, low Nb and Ta concentrations, and low HREE abundances. Indeed, many metasomatized peridotites are characterized by high Nb/Ta ratios (>17.5; Kalfoun et al., 2002; Niu, 2004) compared to depleted mantle peridotites (7-10; Weyer et al., 2003). Furthermore, amphibole would be produced at relatively low melt: rock ratio (e.g., 1:1; Rapp et al., 1999). In contrast, mechanical mixing of the complementary rutile-bearing eclogitic residues with deeper mantle peridotite would develop mantle garnet- and clinopyroxene-rich reservoirs with high Nb and Ta contents but low Nb/Ta ratio. In both cases, mixing or reaction with the peridotite would result in dilution of TiO_2 contents such that rutile would no longer be a primary phase during partial melting of resulting hybrid sources. As such, we speculate that subsequent re-melting of the metasomatized peridotite could have given rise to the high Nb/Ta ratios and low Nb and Ta contents of the >110 Ma basalts while re-melting of the peridotite–eclogite residue mixtures could have given rise to the low Nb/Ta ratios and high Nb and Ta contents of the <110 Ma basalts.

5.2. High Fe/Mn ratios caused by garnet–pyroxenite sources

We now explore the nature of the high Fe/Mn ratios seen in both basaltic suites. To reiterate, partial melting experiments indicate that (1) $D_{Fe/Mn}$ values for both pyroxene (average = 0.91 and 0.65 for opx and cpx, respectively) and garnet (average = 0.45) are <1, but are >1 for olivine (average = 1.35) (Fig. 1), and (2) high Fe/Mn ratios (>60) can be produced by less than 70% partial melting of pyroxenite (Kogiso and Hirschmann, 2001; Pertermann and Hirschmann, 2003a; Keshav et al., 2004; Kogiso et al., 2004), or greater than 50% melting of hydrous peridotite (Gaetani and Grove, 1998; Falloon and Danyushevsky, 2000; Parman and Grove, 2004) (Fig. 1c).

Additional interpretations for the high Fe/Mn ratios of basalts include (1) iron enrichments resulting from core-mantle interaction (Humayun et al., 2004), (2) remelting of previously melted mantle (Lee, 2004), (3) ol accumulation, and (4) fractional crystallization of oxide, ol and cpx. In the context of the Chinese basalts, these four scenarios are unlikely for the following reasons. Core-mantle interaction is unlikely because there is no geologic evidence that the East China basalts were ever associated with deep-seated plumes (Niu, 2005). Furthermore, tungsten isotope ruled out contribution from the Earth's core for mantle plumes (Scherstén et al., 2004). Re-melting of previously melted peridotitic mantle seems unlikely because this would not give rise to coupled OIB-type enrichments and high Fe/Mn. Except for the Luanshishanzi basalts, the <110 Ma basalts have low Ni contents and Mg# (Table 1). Their high Fe/Mn ratios cannot be attributed to ol cumulates. The Luanshishanzi basalts contain abundant low-F_o (<80) ol xenocrysts (5–10%) (Wang et al., 2006). Their high Fe/Mn ratios coupled with high MgO and Ni contents and Mg# could be partially attributed to ol cumulates. The fourth scenario is more difficult to rule out. Fractional crystallization of oxides, ol and cpx could potentially affect Fe/Mn ratios. However, ol and oxide fractionation would decrease Fe/Mn ratio of the melt. Crystal fractionation of cpx, on the other hand, could produce melts with high Fe/Mn ratios, but this would require a high fraction of crystallization (>30–70%) to match the observed Fe/Mn ratios seen in our samples (Fig. 3g). This degree of crystallization is unrealistic considering that our samples have MgO >7.5 wt%. Furthermore, crystal fractionation of cpx would produce melts with positive correlations between Fe/Mn ratios and Yb (Y) contents, but a negative correlation is seen for example in the <110 Ma basalts (Fig. 6b). These observations imply that the high Fe/Mn ratios of the <110 Ma basalts with MgO contents >7.5 wt% did not result from cpx + ol fractionation, but are probably close to the ratios of the primary magma.

Eclogite-related mantle sources associated with recycled oceanic crust have been invoked to account for the generation of some Hawaiian basalts (Hauri, 1996; Kogiso et al., 1998; Gaffney et al., 2005; Huang and Frey, 2005; Sobolev et al., 2005), and Iceland basalts (Korenaga and Kelemen, 2000; Foulger et al., 2005; Thirlwall et al., 2006; Thomas Find et al., 2006; Sigmarsson and Steinthorsson, 2007; Sobolev et al., 2007), both of which have higher Fe/Mn ratios compared with the peridotite melt at the same MnO level (Fig. 1d). To interpret the petrogenesis of the Hawaiian lavas, mixing of melts from peridotite and secondary pyroxenite formed by eclogite-derived melt–peridotite reaction (Sobolev et al., 2005), or mixing of high temperature melts from peridotite and low temperature dacitic melt from garnet pyroxenite (formed from recycled basaltic oceanic crust) (Huang and Frey, 2005) by different physical mechanisms (melt–melt, melt–solid and sold–sold mixing) (Gaffney et al., 2005) were

suggested. Unlike Hawaiian basalts, most of the high Fe/Mn Chinese basalts do not have high Ni, Cr and SiO_2 contents (Fig. 5e and f, Table 1), and thus were not derived from ol-free pyroxenitic sources formed by high-Si melt–peridotite reaction (Sobolev et al., 2005). This can be resolved if the pyroxenitic sources were formed by mechanical mixing of rutile-bearing eclogite and peridotite. Introduction of eclogite into peridotite would result in relative enrichments of cpx and gar, but not consume ol completely. Therefore, olivine together with pyroxene would buffer Ni, Cr and Si at lower levels. Thus, we suggest that the <110 Ma basalts were derived from a cpx- and gar-rich mantle source, which could have been formed by mechanical mixing of rutile-bearing eclogite and peridotite. Such mantle sources can explain well their high Fe/Mn ratios, negative Fe/Mn–Yb (Y) correlations (Fig. 6b) and other major element compositions (Fig. 3). The good positive correlation between Sc and Yb for the <110 Ma basalts (except for those from Caiyuan) is consistent with garnet-rich sources (Fig. 6c). The specific Sc enrichment relative to Yb for those basalts from Caiyuan could result from presence of abundant cpx and ol phenocrysts (10–20%; Wang et al., 2007).

We now discuss the origin of the Fe/Mn ratios characterizing the >110 Ma Mesozoic basalts. Although these basalts have lower Fe/Mn ratios than the <110 Ma basalts, they are still higher than MORB values (Fig. 6d) and values predicted for melting of dry peridotite (Fig. 3g). These observations also suggest pyroxene/garnet-rich mantle sources for the >110 Ma basalts. Although REE patterns and low HREE contents of these >110 Ma basalts demonstrate garnet signature, the negative correlation between Sc and Yb suggests that their mantle sources are pyroxene-dominated because Sc is moderately compatible and Yb is incompatible in cpx (Hart and Dunn, 1993) and opx (Matsui et al., 1977) while both Sc and Yb are highly compatible in gar in equilibrium with basalt (Hauri et al., 1994). Furthermore, the positive correlations between Fe/Mn ratio and Y and HREE are inconsistent with abundant garnet in the source of >110 Ma lavas either (Fig. 6b). These observations suggest that, although garnet may have been present in the mantle sources of the >110 Ma basalts, its proportion is small. The mantle sources for the >110 Ma basalts could be gar-bearing opx-rich pyroxenite or veined peridotite composed of lherzolite and gar-bearing opx-rich pyroxenite, which could have been formed by silicic melt–peridotite reaction (Ringwood, 1974; Rapp et al., 1999; Yaxley, 2000; Liu et al., 2005; Morgan and Liang, 2005). Opx has $D_{Fe/Mn}$ (average = 0.91) higher than cpx (0.65) and gar (0.45), but lower than ol (1.35). Melting of such an opx-rich pyroxenitic source would produce melts with slightly high Fe/Mn ratios and SiO_2 contents but high Ni contents (Kelemen et al., 1998) as shown by the >110 Ma basalts (Figs. 3a, f and 5e). Therefore, we suggest that the >110 Ma basalts were derived from gar-bearing opx-rich pyroxenitic sources.

5.3. Towards a unified model for the Mesozoic and Cenozoic basalts

Coupled with the Late Mesozoic and Cenozoic tectonothermal reactivation, the ancient, cratonic mantle lithosphere of the NCC is believed to have been removed from the base of the eastern block by foundering, stretching or thermal/chemical erosion of the deep lithosphere due to upwelling asthenosphere (Menzies et al., 1993; Griffin et al., 1998; Xu, 2001; Gao et al., 2002; Wu et al., 2003; Gao et al., 2004; Rudnick et al., 2004; Wu et al., 2005; Wu et al., 2006; Menzies et al., 2007). Thermo-chemical erosion of the Archean lithospheric mantle by upwelling asthenosphere (Menzies et al., 1993; Griffin et al., 1998; Menzies et al., 2007) cannot well explain the production of adakitic/TTG lavas from foundered NCC crust prior to basaltic magmatism (Gao et al., 2004), the evolved Sr–Nd isotopic compositions of the Mesozoic basalts and the entrainment of fragments of the Archean mantle and lower crust by high-Mg diorites of the NCC crustal origin (Chen and Zhou, 2005; Xu et al., 2006). High-Mg# adakitic lavas in Eastern China suggest that the mafic lower continental crust had been recycled into the convecting mantle during the Mesozoic lithospheric thinning (Gao et al., 2001; Gao et al., 2004; Wu et al., 2005). Delamination and foundering of the deep lithosphere (lower crust plus lithospheric mantle) seem more reasonable to explain the above observations (Gao et al., 2001; Gao et al., 2004; Wu et al., 2005), which could have induced widespread melt–peridotite reaction (Chen and Zhou, 2005; Liu et al., 2005) and the Mesozoic picrites and basalts with evolved Nd, Sr and Os isotopic compositions (Gao et al., 2008), and resulted in enrichment of recycled eclogitic components in the Cenozoic mantle beneath Eastern China. Preferential partial melting of recycled mafic crustal rocks could lead to three types of mixing/reaction associated with Mesozoic lithospheric thinning: (1) silicic melt–peridotite reaction by equilibrium infiltration, (2) mechanical mixing of peridotite and silicic melt by injection and freezing of melts into cold lithospheric mantle, and (3) solid-state mechanical mixing of peridotite and the eclogitic residues after silicic melt extraction. Each of these scenarios is discussed below. Trace elemental and Sr–Nd isotopic compositions of the melts formed by these three types of mixing/reaction were calculated (Fig. 8).

Reaction between peridotite and infiltrating silicic melt is thought to produce harzburgite or orthopyroxene-rich pyroxenite in equilibrium with high-Mg# melts (Ringwood, 1974; Kelemen et al., 1992; Varfalvy et al., 1997; Kelemen et al., 1998; Rapp et al., 1999; Yaxley, 2000). The trace elemental and isotopic compositions of the melt/peridotite reaction zones depend on composition of the melt as well as equilibration with the mineral assemblage, that is, instead of simple mechanical mixing of chemical components, the trace element compositions are buffered by the mineral assemblage and melt (Kelemen, 1986). We modeled a two stage process for production of the >110 Ma basalts, in which reaction between silicic melt and peridotite produces a pyroxenite, and then later melting of pyroxenite and peridotite in varying proportions. Our model calculations suggest that, although opx-rich pyroxenite formed by the melt–rock reaction would not be significantly enriched in highly incompatible elements, low degree melting (~1%) of pyroxenite + peridotite mixture could produce high Nb/Ta ratios and trace element patterns of >110 Ma basalts (Figs. 6d and 8a). Moreover, Sr–Nd isotopic compositions of the

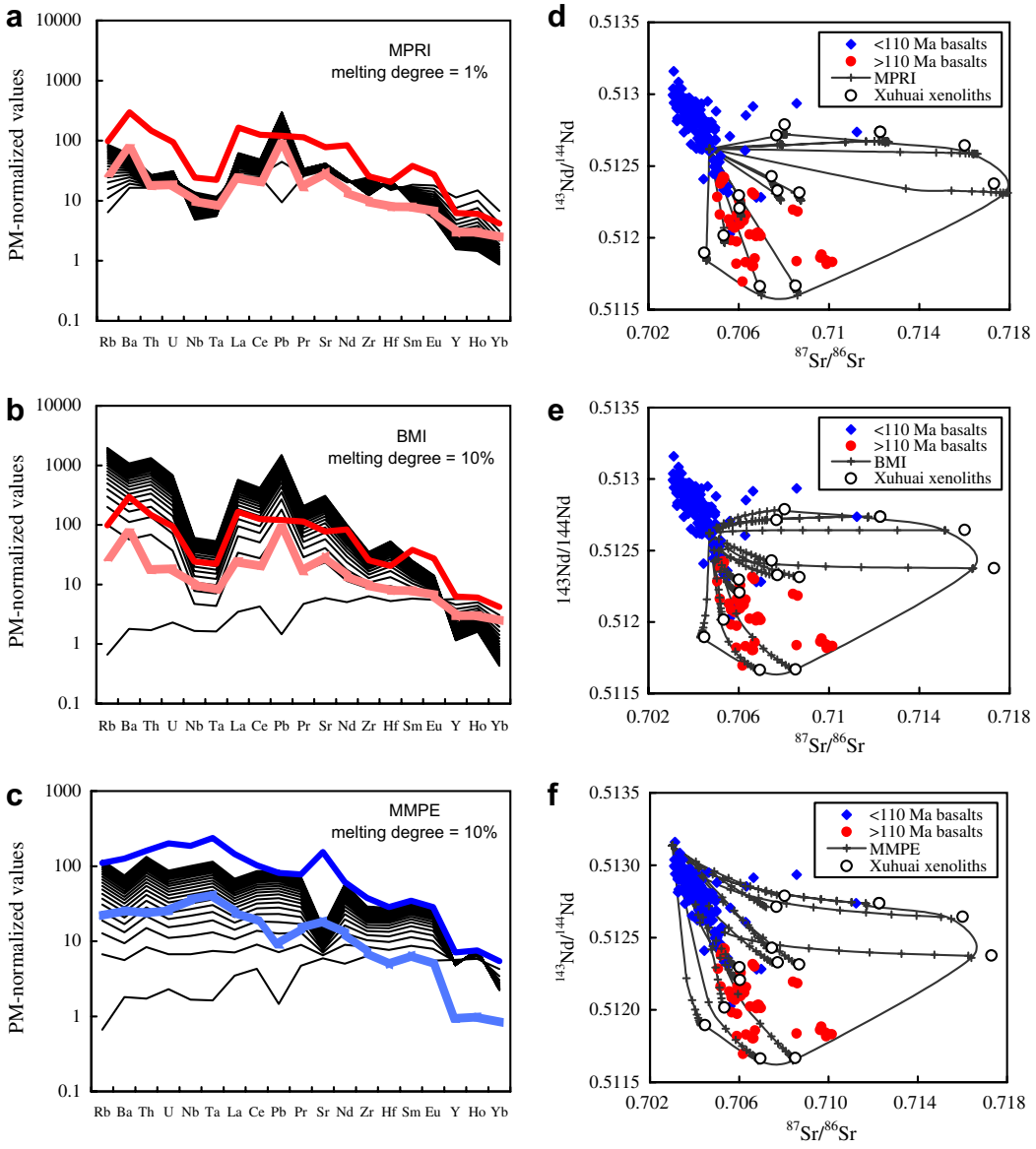

Fig. 8. (a) Partial melts (melting degree = 1%) of mixture formed by melt–peridotite reaction by infiltration (MPRI). Silicic melt was assumed to be produced by 10% partial melting of recycled lower continental crust. (b) Partial melts (melting degree = 10%) of mixture formed by peridotite-melt reaction by injection (BMI). (c) Partial melts (melting degree = 10%) of mechanical mixtures of peridotite and residual eclogite (MMPE). Peridotite was assumed to be composed of 65%ol + 15%cpx + 15%opx + 5%sp, and converted to pyroxenite (40%cpx + 30%opx + 30%gar) after addition of eclogite melt. Partial melts were simply calculated according to batch melting mode. Partition coefficients and trace element compositions of end members used in the calculations are listed in Table 2. Each thin line represents a 10% increment of secondary pyroxenite for MPRI and BMI, and eclogite for MMPE. The thick lines are maximum and minimum values of the >110 Ma basalts in (a and b) and <110 Ma basalts in (c). PM values are from McDonough and Sun (1995). (c–f) Sr–Nd isotopic compositions of partial melts of MPRI, BMI and MMPE. Model calculations were conducted using the Xuhuai eclogite/garnet clinopyroxenite xenoliths (Wang et al., 2005) for the composition of recycled lower continental crust. Nd and Sr isotopic compositions of the >110 Ma mantle peridotites were represented by harzburgite xenoliths with the most radiogenic Nd from the 133 Ma Laiwu pyroxene-diorite ($^{143}Nd/^{144}Nd = 0.51263$; Xu et al., 2003) and the average $^{87}Sr/^{86}Sr$ of continental lithospheric mantle (0.7047, Pearson and Nowell, 2002). Nd and Sr isotopic compositions of the <110 Ma mantle peridotites were represented by lherzolite xenoliths from the 22.8 Ma Hannuoba basalt ($^{143}Nd/^{144}Nd = 0.51318$, $^{87}Sr/^{86}Sr = 0.70316$) (Song and Frey, 1989). Sr and Nd isotopic compositions of the basalts were collected from literatures (Zhou and Armstrong, 1982; Peng et al., 1986; Liu et al., 1989; Song et al., 1990; Chen, 1992; Chen et al., 1992; Wang and Xie, 1992; Xie and Wang, 1992; Zhang and Chen, 1992; Zhang et al., 1992; Zhi and Feng, 1992; Zhou et al., 1992; Liu et al., 1995b; Cong et al., 1996; Zhang et al., 1998; Zhou et al., 2001; Zhang et al., 2002, 2003; Zhang and Zheng, 2003). Each plus on the lines represents a 10% increment of secondary pyroxenite for MPRI and BMI, and eclogite for MMPE.

>110 Ma basalts fall within the melt range calculated using the composition of the Xuhuai eclogite/garnet–clinopyroxenite xenoliths as the recycled continental crust component (Fig. 8d).

As an alternative, involving larger degree melts of eclogite, we modeled melting of mixtures of "crystallized eclogite melt" and peridotite, without the initial melt–peridotite reaction step. Injection of silicic melts into cold peridotite, in the form of a dike or grain boundary melt as well as melt–peridotite reaction, can be approximated as simple melt–solid mixing in a closed system. In this case, the effects of reaction between melt and peridotite are considered negligible. Because the eclogite-derived melt is enriched in highly incompatible elements compared to the peridotite wallrock, addition of a few percent melt can substantially change the incompatible element and Sr–Nd isotopic compositions of the mixture. Partial melts of such mixtures at a relatively high melting degree (10%) show not only the island arc-type trace element compositions (Fig. 8b) and high Nb/Ta ratios (Fig. 6d), but also Sr–Nd isotopic compositions of the >110 Ma basalts (Fig. 8e). Such process can explain the peridotite melt-like major elements of the >110 Ma basalts as well (Fig. 3).

It is worth noting that, 40–60 wt% melt is required to convert all olivine in typical lherzolite into pyroxene + garnet (Sobolev et al., 2005), while a small proportion of melt added to peridotite would not completely consume olivine in the mixture. Therefore, melting of such ol-bearing mixture would not fractionate Ni from Cr because Ni would still be significantly buffered by olivine, in contrast to the fractionation of Ni from Cr observed in high-Mg# Hawaiian basalts (Fig. 5) that are thought to be derived from an olivine-free mantle (Sobolev et al., 2005).

Finally, a third possibility is that the sources of the <110 Ma basalts are mechanical mixtures of rutile-bearing eclogitic residues with deeper mantle peridotite. This would produce gar- and cpx-rich mantle reservoirs with high Nb and Ta contents but low Nb/Ta ratios. Melting of such mixtures to the point of rutile exhaustion (due to increasing temperature) would yield melts with low Nb/Ta ratios and high Fe/Mn ratios, coupled with OIB-type trace element features. Except for Sr, the other elements and Nb/Ta and Fe/Mn ratios can be well modeled by this scenario (Figs. 6d and 8c). The Sr anomaly may arise because we did not account for apatite, a common mineral in ultra-high pressure eclogites. Sr is highly compatible in apatite, and would be preferentially retained in the eclogite residue if apatite was a residual phase during the proposed first stage of small degree melting. This is consistent with the observations that some >110 Ma basalts show depletion in *P* while most <110 Ma basalts show enrichment in *P* (Fig. 4). Our calculations suggest that 30–100% eclogite/garnet clinopyroxenite is required to produce the OIB-type trace element compositions of the <110 Ma basalts for 10% partial melting (Fig. 8c). Such a high eclogite/garnet clinopyroxenite proportion could be attributed to low solidi for pyroxenite compared with peridotite. At a given pressure, eclogite–garnet clinopyroxenite will be preferentially sampled during partial melting, particularly at low melt fraction. Therefore, the net proportion of pyroxenite in the melted part of the mixture could be significantly higher than that in the whole mixture. The highly variable Sr–Nd isotopic compositions of the <110 Ma basalts can be produced by partial melting of such a mixture using the Xuhuai eclogite/garnet clinopyroxenite xenoliths as the recycled continental crust (Fig. 8f).

To summarize, based on Nb/Ta and Fe/Mn ratios, trace element patterns and Nd–Sr isotopes we propose a unified model for the Mesozoic and Cenozoic basalts. In this model, we suggest that the sources of the >110 Ma basalts were gar-bearing opx-rich pyroxenite or pyroxenite-veined peridotite formed by reaction and/or mixing between peridotite and eclogite-derived felsic melts, while the sources of the <110 Ma basalts were mechanical mixtures of peridotite and eclogitic residues formed by the earlier stage of felsic melt extraction. The differentiated Nb/Ta and high Fe/Mn ratios of the basalts are fingerprints of the Mesozoic delamination and foundering of deep lithosphere (lower crust plus lithospheric mantle) (Gao et al., 2004; Wu et al., 2005; Xu et al., 2002). Those composite xenoliths formed by melt–peridotite reactions found in the Cenozoic basalts (Liu et al., 2005) and Mesozoic high-Mg diorite (Chen and Zhou, 2005) could have sampled the Mesozoic pyroxenite-veined peridotite. Xu et al. (2006) reported eclogite and garnet clinopyroxenite xenoliths found in the high-Mg adakites. Although eclogite xenoliths is not found in Cenozoic basalts, some cpx phenocrysts in the Cenozoic basalts show the same reverse zoning (i.e., high FeO, MnO, Na_2O, and Al_2O_3 contents in the core) (Wang et al., 2007) as those in the late Jurassic high-Mg adakites (Gao et al., 2004), and suggest presence of crustal pyroxenite in the mantle sources. The absence of eclogite xenoliths in the Cenozoic basalts could be attributed to high degree melting due to their lower solidus than peridotite (Yasuda et al., 1994; Hirschmann and Stolper, 1996; Hirschmann, 2000; Keshav et al., 2004) and high dissolution rate of cpx and gar in alkali basalts at low pressure (Brearley and Scarfe, 1986; Edwards and Russell, 1996).

Extensive contributions of pyroxenites in mid-ocean ridge basalts, ocean island and continental basalts, and komatiites have been suggested by Sobolev et al. (2007). The model suggested for the <110 Ma Chinese basalts could be applicable to other cratons that suffered lithospheric thinning. For example, the Cenozoic basalts from the Basin and Range Province also have high Fe/Mn ratio coupled with OIB-type trace element signatures (Feuerbach et al., 1993).

6. CONCLUSIONS

Fe/Mn and Nb/Ta ratios of basalts are tracers that can differentiate effectively melts of recycled mafic crustal lithologies from peridotitic melts. $D_{Fe/Mn}$ values for both pyroxene (average = 0.95 and 0.65 for opx and cpx, respectively) and gar (average = 0.69) are <1, but are >1 for ol (average = 1.31). Statistic summary of previous experiments indicates that, for less than 50% melting, high Fe/Mn ratios (>60) in "primitive" basalts point to an eclogite/pyroxenite source, while lower values suggest a peridotite source. Rutile strongly partitions Nb and Ta from melt ($D_{Nb,\,Ta}^{rutile/melt} \gg 1$), and effectively fractionates Nb from Ta, such that melts in equilibrium with rutile are characterized by high Nb/Ta ratios. As a result, initial melts of rutile-bearing eclogite should have relatively high Nb/Ta ratios.

Progressive melting of these eclogites would exhaust rutile, thereby resulting in melts with low Nb/Ta ratios inherited from earlier melt depletion. By contrast, melts of rutile-free peridotitic mantle unaffected by recycled crust would be characterized by Nb/Ta ratios close to the primitive mantle value.

As an example, we applied these tools to investigate the origin of Mesozoic and Cenozoic basalts from Eastern China. High Fe/Mn ratios, negative correlations of Fe/Mn–Yb (Y) and positive correlation of Sc–Yb suggest cpx/gar-rich mantle sources for the <110 Ma basalts. Integration of the garnet signature (i.e., low HREE contents), high Fe/Mn ratios (mostly higher than peridotite melt) and positive correlations of Fe/Mn–Yb (Y) and negative correlation of Sc–Yb suggests gar-bearing opx-rich mantle sources for the >110 Ma basalts. Combining this reasoning with data on Sr–Nd isotopes, we outline a unified model to explain the relatively high Fe/Mn and differentiated Nb/Ta ratios and contrasting trace element patterns of the >110 Ma basalts and <110 Ma basalts. We suggest that preferential melting of recycled ancient lower continental crust during Mesozoic lithospheric thinning resulted in (1) peridotite-melt reactive mixing that formed the opx-rich mantle sources for the >110 Ma basalts and (2) mechanical mixing between peridotite and rutile-bearing eclogitic residue that formed the cpx- and gar-rich mantle sources for the <110 Ma basalts. The high Fe/Mn ratios and contrasting Nb/Ta ratios of the >110 Ma basalts and <110 Ma basalts could be a signature of the Mesozoic lower crustal recycling in Eastern China.

ACKNOWLEDGMENTS

Dr. Tetsu Kogiso, Yaoling Niu, Michele Lustrino, Matthias Barth and one anonymous reviewer are thanked for detailed comments that helped us to improve the manuscript. Dr. Cin-Ty Lee is thanked for polishing the original manuscript. Dr. Menzies is thanked for the editorial work. This work was supported by the National Natural Science Foundation of China (Grants 40521001, 40673026, 90714010, 40673019), the Ministry of Education of China as well as the Ministry of the Foreign Affairs of China (IRT0441, NCET-05-0664, B07039 and 20040183065). Kelemen was supported in part by NSF Research Grants OCE 0426160 and OCE 0405572. Gao C.G., Zhang B.H. and Tong C.L. were thanked for their work in ICP-MS analyses.

REFERENCES

Allégre J.-C. and Turcotte D. L. (1986) Implications of a two-component marble-cake mantle. *Nature* **323**, 123–127.

Anderson D. L. (1989) *Theory of the Earth*. Blackwell Sci. Publ.

Anderson D. L. (2005) Large igneous provinces, delamination, and fertile mantle. *Elements* **1**(5), 271–275.

Anderson D. L. (2006) Speculations on the nature and cause of mantle heterogeneity. *Tectonophysics* **416**(1–4), 7–22.

Ayers J. C. and Watson E. B. (1991) Solubility of apatite, monazite, zircon, and rutile in supercritical aqueous fluids with implications for subduction zone geochemistry. *Phil. Trans. R. Soc.* **335**, 365–375.

Baker M. B. and Stolper E. M. (1994) Determining the composition of high-pressure mantle melts using diamond aggregates. *Geochim. Cosmochim. Acta* **58**(13), 2811–2827.

Barth M. G., Foley S. F. and Horn I. (2002) Partial melting in Archean subduction zones: constraints from experimentally determined trace element partition coefficients between eclogitic minerals and tonalitic melts under upper mantle conditions. *Precambrian Res.*(113), 323–340.

Beattie P. (1993) The effect of partial melting of spinel peridotite on uranium series disequilibria: constraints from partitioning studies. *Earth Planet. Sci. Lett.* **177**, 379–391.

Brearley M. and Scarfe C. M. (1986) Dissolution rates of upper mantle minerals in an alkali basalt melt at high pressure: an experimental study and implications for ultramafic xenolith survival. *J. Petrology* **27**(5), 1157–1182.

Brenan J. M., Shaw H. F., Phinney D. L. and Ryerson F. J. (1994) Rutile-aqueous fluid partitioning of Nb, Ta, Hf, Zr, U and Th: implications for high field strength element depletions in Island-arc basalts. *Earth Planet. Sci. Lett.* **128**, 327–339.

Chauvel C., McDonough W., Guille G., Maury R. and Duncan R. (1997) Contrasting old and young volcanism in Rurutu Island, Austral chain. *Chem. Geol.* **139**(1–4), 125–143.

Chen D. G. (1992) The geochemistry of Cenozoic basalt at the middle-south segment of Tanlu fault zone. In *The Age and Geochemistry of Cenozoic Volcanic Rock in China* (ed. R. X. Liu). Seismic Press, pp. 171–209.

Chen L. H. and Zhou X. H. (2005) Subduction-related metasomatism in the thinning lithosphere: evidence from a composite duniteorthopyroxenite xenolith entrained in Mesozoic Laiwu high-Mg diorite, North China Craton. *Geochem. Geophys. Geosyst.* **6**(Q06008). doi:10.1029/2005GC000938.

Chen W. J., Li D. M., Li Q., Shen S. W., Liang H. D., Zhou X. H., Liu R. X., Wang X., Liu X. T. and Zheng J. W. (1992) The age and geochemistry of basin basalt at Xialiaohe rift. In *The Age and Geochemistry of Cenozoic Volcanic Rock in China* (ed. R. X. Liu). Seismic Press, pp. 44–80.

Chi J. (1987) *The study of Cenozoic basalts and the upper mantle beneath Eastern China (attachment: Kimberlite)*. China University of Geosciencs Press.

Cong B. L., Wang Q. C., Zhang H. Z., Yan X. and Jiang L. L. (1996) Petrogenesis of Cenozoic volcanic rocks in Hefei basin, China. *Acta Petrol. Sin. (in Chinese with English Abs.)* **12**(3), 370–381.

Cordery M. J., Davies G. F. and Campbell I. H. (1997) Genesis of flood basalts from eclogite-bearing mantle plumes. *J. Geophys. Res. Solid Earth* **102**(B9), 20179–20197.

Dasgupta R., Hirschmann M. M. and Withers A. C. (2004) Deep global cycling of carbon constrained by the solidus of anhydrous, carbonated eclogite under upper mantle conditions. *Earth Planet. Sci. Lett.* **227**, 73–85.

Donnelly K. E., Goldstein S. L., Langmuir C. H. and Spiegelman M. (2004) Origin of enriched ocean ridge basalts and implications for mantle dynamics. *Earth Planet. Sci. Lett.* **226**(3–4), 347–366.

Dunn T. and Sen C. (1994) Mineral/matrix partition coefficients for orthopyroxene, plagioclase, and olivine in basaltic to andesitic systems: a combined analytical and experimental study. *Geochim. Cosmochim. Acta* **58**(2), 717–733.

Edwards B. R. and Russell J. K. (1996) A review and analysis of silicate mineral dissolution experiments in natural silicate melts. *Chem. Geol.* **130**(3–4), 233–245.

Eiler J. M., Schiano P., Kitchen N. and Stolper E. M. (2000) Oxygen-isotope evidence for recycled crust in the sources of mid-ocean-ridge basalts. *Nature* **403**, 530–534.

Elliott T., Thomas A., Jeffcoate A. and Niu Y. (2006) Lithium isotope evidence for subduction-enriched mantle in the source of mid-ocean-ridge basalts. *Nature* **443**(7111), 565–568.

Escrig S., Capmas F., Dupré B. and Allégre C. J. (2004) Osmium isotopic constraints on the nature of the DUPAL anomaly from Indian mid-ocean-ridge basalts. *Nature* **43**, 59–63.

Falloon T. J. and Danyushevsky L. V. (2000) Melting of refractory mantle at 1.5, 2 and 2.5 GPa under anhydrous and H_2O-undersaturated conditions: implications for the petrogenesis of high-Ca boninites and the influence of subduction components on mantle melting. *J. Petrol.* **41**(2), 257–283.

Falloon T. J., Green D. H., Danyushevsky L. V. and Faul U. H. (1999) Peridotite melting at 1.0 and 1.5 GPa: an experimental evaluation of techniques using diamond aggregates and mineral mixes for determination of near-solidus melts. *J. Petrol.* **40**(9), 1343–1375.

Feuerbach D. L., Smith E. I., Walker J. D. and Tangeman J. A. (1993) The role of the mantle during crustal extension: constriants from geochemistry of volcanic rocks in the Lake Mead area, Nevada and Arizona. *Geol. Soc. Am. Bull.* **105**, 1561–1575.

Foley S. F., Barth M. G. and Jenner G. A. (2000) Rutile/melt partition coefficients for trace elements and an assessment of the influence of rutile on the trace element characteristics of subduction zone magmas. *Geochim. Cosmochim. Acta* **64**(5), 933–938.

Foulger G. R., Natland J. H. and Anderson D. L. (2005) A source for Icelandic magmas in remelted Iapetus crust. *J. Volcanol. Geotherm. Res.* **141**(1–2), 23–44.

Gaetani G. and Grove T. (1998) The influence of water on melting of mantle peridotite. *Contrib. Mineral. Petrol.* **131**, 323–346.

Gaffney A. M., Nelson B. K. and Blichert-Toft J. (2004) Geochemical constraints on the role of oceanic lithosphere in intra-volcano heterogeneity at West Maui, Hawaii. *J. Petrol.* **45**(8), 1663–1687.

Gaffney A. M., Nelson B. K. and Blichert-Toft J. (2005) Melting in the Hawaiian plume at 1–2 Ma as recorded at Maui Nui: the role of eclogite, peridotite, and source mixing. *Geochem. Geophys. Geosyst.* **6**(Q10L11). doi:10.1029/2005GC000927.

Gao S., Liu Y. S., Yuan H. L. and Ling W. L. (2001) Geochemistry of Jurassic-Cretaceous high-Mg adakite from North China Craton suggests delamination of eclogitic lower crust. In *Symposium on adakite-like rocks and their geodynamic significance*.

Gao S., Rudnick R. L., Carlson R. W., McDonough W. F. and Liu Y. S. (2002) Re–Os evidence for replacement of ancient mantle lithosphere beneath the North China craton. *Earth Planet. Sci. Lett.* **198**, 307–322.

Gao S., Rudnick R. L., Xu W. -L., Yuan H. -L., Liu Y. -S., Walker R. J., Puchtel I., Liu X., Huang H., Wang X. -R. and Yang J. (2008) Recycling deep cratonic lithosphere and generation of intraplate magmatism in the North China Craton. *Earth Planet. Sci. Lett.*, in press, doi:10.1016/j.epsl.2008.03.008.

Gao S., Rudnick R. L., Yuan H. L., Liu X. M., Liu Y. S., Xu W. L., Ling W. L., Ayers J., Wang X. C. and Wang Q. H. (2004) Recycling lower continental crust in the North China craton. *Nature* **432**, 892–897.

Green T. H., Adam J. and Site S. H. (1993) Proton microprobe determined trace element partition coefficients between pargasite, augite and silicate or carbonatitic melts. *EOS* **74**, 340.

Green T. H. and Pearson N. J. (1986) Ti-rich accessory phase saturation in hydrous mafic–felsic compositions at high P,T. *Chem. Geol.* **54**(3–4), 185–201.

Green T. H. and Pearson N. J. (1987) An experimental study of Nb and Ta partitioning between Ti-rich minerals and silicate liquids at high pressure and temperature. *Geochim. Cosmochim. Acta* **51**, 55–62.

Griffin W. L., Zhang A., O'Reilly S. Y. and Ryan C. G. (1998) Phanerozoic evolution of the lithosphere beneath the Sino-Korean Craton. In *Mantle Dynamics and Plate Interactions in East Asia*, vol. 27 (eds. M. Flower, S. L. Chung, C. H. Lo and T. Y. Lee), pp. 107–126. Geodynamics Volume. American Geophysical Union.

Hart S. R. and Dunn T. (1993) Experimental cpx/melt partitioning of 24 trace elements. *Contrib. Mineral. Petrol.* **113**, 1–8.

Hauri E. H. (1996) Major-element variability in the Hawaiian mantle plume. *Nature* **382**, 415–419.

Hauri E. H., Wagner T. P. and Grove T. L. (1994) Experimental and natural partitioning of Th, U, Pb and other trace elements between garnet, clinopyroxene and basaltic melts. *Chem. Geol.* **117**, 149–166.

Herzberg C. (2006) Petrology and thermal structure of the Hawaiian plume from Mauna Kea volcano. *Nature* **444**(7119), 605–609.

Herzberg C. T., Fyfe W. S. and Carr M. J. (1983) Density constraints on the formation of the continental Moho and crust. *Contrib. Mineral. Petrol.* **84**(1–5).

Hirose K. and Kushiro I. (1993) Partial melting of dry peridotites at high pressures: determination of compositions of melts segregated from peridotite using aggregates of diamond. *Earth Planet. Sci. Lett.* **114**(4), 477–489.

Hirschmann M. M. (2000) Mantle solidus: experimental constraints and the effect of peridotite composition. In *Geochem. Geophys. Geosyst.*, vol. 1, pp. Paper No. 2000GC000070.

Hirschmann M. M., Kogiso T., Baker M. B. and Stolper E. M. (2003) Alkalic magmas generated by partial melting of garnet pyroxenite. *Geology* **31**, 481–484.

Hirschmann M. M. and Stolper E. (1996) A possible role for garnet pyroxenite in the origin of the "garnet signature" in MORB. *Contrib. Mineral. Petrol.* **124**, 185–208.

Hsu C. N. and Chen J. C. (1998) Geochemistry of late Cenozoic basalts from Wudalianchi and Jingpohu areas, Heilongjiang Province, northeast China. *J. Asian Earth Sci.* **16**(4), 385–405.

Huang S. and Frey F. A. (2005) Recycled oceanic crust in the Hawaiian Plume: evidence from temporal geochemical variations within the Koolau Shield. *Contrib. Mineral. Petrol.* **149**(5), 556–575.

Humayun M., Qiu L. and Norman M. D. (2004) Geochemical evidence for excess iron in the mantle beneath Hawaii. *Science* **306**, 91–94.

Jacob D. E. (2004) Nature and origin of eclogite xenoliths from kimberlites. *Lithos* **77**, 295–316.

Kalfoun F., Ionov D. and Merlet C. (2002) HFSE residence and Nb/Ta ratios in metasomatised, rutile-bearing mantle peridotites. *Earth Planet. Sci. Lett.* **199**(1–2), 49–65.

Kay R. W. (1978) Aleutian magnesian andesites: melts from subducted Pacific ocean crust. *J. Volcanol. Geotherm. Res.* **4**(1–2), 117–132.

Kay R. W. and Kay S. M. (1991) Creation and destruction of lower continental crust. *Geol. Rundsch.* **80**, 259–278.

Keleman P. B. and Dunn J. T. (1992) Depletion of Nb relative to other highly incompatible elements by melt/rock reaction in the upper mantle. *EOS* **73**, 656–657.

Kelemen P. B. (1986) Assimilation of ultramafic rock in subduction-related magmatic arcs. *J. Geol.* **94**, 829–843.

Kelemen P. B. (1995) Genesis of high Mg# andesites and the continental crust. *Contrib. Mineral. Petrol.* **120**(1), 1–19.

Kelemen P. B., Dick H. J. B. and Quick J. E. (1992) Formation of harzburgite by pervasive melt/rock reaction in the upper mantle. *Nature* **358**, 635–641.

Kelemen P. B., Hanghoj K. and Greene A. R. (2003) One view of the geochemistry of subduction-related magmatic arcs, with emphasis on primitive andesite and lower crust. In *The Crust*, vol. 3 (ed. R. L. Rudnick). Elsevier, pp. 593–659.

Kelemen P. B., Hart S. R. and Bernstein S. (1998) Silica enrichment in the continental upper mantle via melt/rock reaction. *Earth Planet. Sci. Lett.* **164**(1–2), 387–406.

Kelemen P. B., Shimizu N. and Dunn D. (1993) Relative depletion of niobium in some arc magmas and the continental crust; partitioning of K, Nb, La and Ce during melt/rock reaction in the upper mantle. *Earth Planet. Sci. Lett.* **120**, 111–134.

Keshav S., Gudfinnsson G. H., Sen G. and Fei Y.-W. (2004) High-pressure melting experiments on garnet clinopyroxenite and the alkalic to tholeiitic transition in ocean-island basalts. *Earth Planet. Sci. Lett.* **223**, 365–379.

Kessel R., Schmidt M. W., Ulmer P. and Pettke T. (2005a) Trace element signature of subduction-zone fluids, melts and supercritical liquids at 120–180 km depth. *Nature* **437**(7059), 724–727.

Kessel R., Ulmer P., Pettke T., Schmidt M. W. and Thompson A. B. (2005b) The water-basalt system at 4 to 6 GPa: phase relations and second critical endpoint in a K-free eclogite at 700 to 1400 °C. *Earth Planet. Sci. Lett.* **237**(3–4), 873–892.

Klemme S., Blundy J. D. and Wood B. D. (2002) Experimental constraints on major and trace element partitioning during partial melting of eclogite. *Geochim. Cosmochim. Acta* **66**, 3109–3123.

Klemme S., Gunther D., Hametner K., Prowatke S. and Zack T. (2006) The partitioning of trace elements between ilmenite, ulvospinel, armalcolite and silicate melts with implications for the early differentiation of the moon. *Chem. Geol.* **234**(3–4), 251–263.

Klemme S., Prowatke S., Hametner K. and Günther D. (2005) Partitioning of trace elements between rutile and silicate melts: implications for subduction zones. *Geochim. Cosmochim. Acta* **69**(9), 2361–2371.

Kogiso T., Hirose K. and Takahashi E. (1998) Melting experiments on homogeneous mixtures of peridotite and basalt: application to the genesis of ocean island basalts. *Earth Planet. Sci. Lett.* **162**, 45–61.

Kogiso T. and Hirschmann M. M. (2001) Experimental study of clinopyroxenite partial melting and the origin of ultra-calcic melt inclusions. *Contrib. Mineral. Petrol.* **142**, 347–360.

Kogiso T. and Hirschmann M. M. (2006) Partial melting experiments of bimineralic eclogite and the role of recycled mafic oceanic crust in the genesis of ocean island basalts. *Earth Planet. Sci. Lett.* **249**(3–4), 188–199.

Kogiso T., Hirschmann M. M. and Frost D. J. (2003) High-pressure partial melting of garnet pyroxenite: possible mafic lithologies in the source of ocean island basalts. *Earth Planet. Sci. Lett.* **216**, 603–617.

Kogiso T., Hirschmann M. M. and Pertermann M. (2004) High-pressure partial melting of mafic lithologies in the mantle. *J. Petrol.* **45**(12), 2407–2422.

Kogiso T., Tatsumi Y. and Nakano S. (1997) Trace element transport during dehydration processes in the subducted oceanic crust: 1. Experiments and implications for the origin of ocean island basalts. *Earth Planet. Sci. Lett.* **148**, 193–205.

Korenaga J. and Kelemen P. B. (2000) Major element heterogeneity in the mantle source of the North Atlantic igneous province. *Earth Planet. Sci. Lett.* **184**(1), 251–268.

Laporte D., Toplis M. J., Seyler M. and Devidal J. M. (2004) A new experimental technique for extracting liquids from peridotite at very low degrees of melting: application to partial melting of depleted peridotite. *Contrib. Mineral. Petrol.* **146**, 463–484.

Lassiter J. C., Hauri E. H., Reiners P. W. and Garcia M. O. (2000) Generation of Hawaiian post-erosional lavas by melting of a mixed lherzolite/pyroxenite source. *Earth Planet. Sci. Lett.* **178**(3–4), 269–284.

Lee C. T. (2004) Are Earth's core and mantle on speaking terms? *Science* **306**, 64–65.

Lee C. T. A., Cheng X. and Horodyskyj U. (2006) The development and refinement of continental arcs by primary basaltic magmatism, garnet pyroxenite accumulation, basaltic recharge and delamination: insights from the Sierra Nevada, California. *Contrib. Mineral. Petrol.* **151**, 222–242.

Liu B. L., Chen Y. W. and Zhu B. Q. (1989) Origin of Cenozoic basalts from Jinbohu, northeast China and chemical characteristics of their mantle source—Sr–Pb isotope and trace element evidence. *Geochimica* **18**(1), 9–19.

Liu C. Q., Xie G. H. and Masuda A. (1995a) Geochemistry of Cenozoic basalts from Eastern China I. major element and trace element compositions: petrogenesis and characteristics of mantle source. *Geochimica* **24**(1), 1–19.

Liu C. Q., Xie G. H. and Masuda A. (1995b) Geochemistry of Cenozoic basalts from Eastern China: (II) Sr, Nd and Ce isotopic compositions. *Geochimica* **24**(3), 203–214.

Liu D. Y., Nutman A. P., Compston W., Wu J. S. and Shen Q. H. (1992a) Remnants of >3800 Ma crust in the Chinese part of the Sino-Korean craton. *Geology* **20**, 339–342.

Liu R. X., Chen W. J., Sun J. Z. and Li D. M. (1992b) The K–Ar age and tectonic environment of Cenozoic volcanic rock in China. In *The Age and Geochemistry of Cenozoic Volcanic Rock in China* (ed. R. X. Liu). Seismic Press, pp. 1–43.

Liu Y. S., Gao S., Jin S. Y., Hu S. H., Sun M., Zhao Z. B. and Feng J. L. (2001) Geochemistry and petrogenesis of lower crustal xenoliths from Hannuoba, North China: implications for the continental lower crustal composition and evolution at convergent margin. *Geochim. Cosmochim. Acta* **65**(15), 2589–2604.

Liu Y. S., Gao S., Lee C.-T. A., Hu S. H., Liu X. M. and Yuan H. L. (2005) Melt–peridotite interactions: links between garnet pyroxenite and high-Mg# signature of continental crust. *Earth Planet. Sci. Lett.* **234**(1–2), 39–57.

Liu Y. S., Gao S., Yuan H. L., Zhou L., Liu X. M., Wang X. C., Hu Z. C. and Wang L. S. (2004) U–Pb zircon ages and Nd, Sr, and Pb isotopes of lower crustal xenoliths from North China Craton: insights on evolution of lower continental crust. *Chem. Geol.* **211**(1–2), 87–109.

Lustrino M. (2005) How the delamination and detachment of lower crust can influence basaltic magmatism. *Earth Sci. Rev.* **72**(1–2), 21–38.

Lustrino M. and Dallai L. (2003) On the origin of EM-I end-member. *N. Jahrb. Miner. Abh.* **179**, 85–100.

Lustrino M., Melluso L. and Morra V. (2000) The role of lower continental crust and lithospheric mantle in the genesis of Plio-Pleistocene volcanic rocks from Sardinia (Italy). *Earth Planet. Sci. Lett.* **180**, 259–270.

Lustrino M., Melluso L. and Morra V. (2007) The geochemical peculiarity of "Plio-Quaternary" volcanic rocks of Sardinia in the circum-Mediterranean area. In *Cenozoic Volcanism in the Mediterranean Area*, vol. 418 (eds. L. Beccaluva, G. Bianchini and M. Wilson). Geological Society of America Special Paper, pp. 277–301.

Matsui Y., Onuma N., Nagasawa H., Higuchi H. and Banno S. (1977) Crystal structure control in trace element partition between crystal and magma. *Tectonics* **100**, 315–324.

McDonough W. F. and Sun S. S. (1995) The composition of the earth. *Chem. Geol.* **120**, 223–253.

McKenzie D. A. N. and O'Nions R. K. (1991) Partial melt distributions from inversion of rare earth element concentrations. *J. Petrol.* **32**(5), 1021–1091.

Meibom A. and Anderson D. L. (2003) The statistical upper mantle assemblage. *Earth Planet. Sci. Lett.* **217**, 123–139.

Menzies M., Xu Y., Zhang H. and Fan W. (2007) Integration of geology, geophysics and geochemistry: a key to understanding the North China Craton. *Lithos* **96**(1–2), 1–21.

Menzies M. A., Fan W. M. and Zhang M. (1993) Paleozoic and Cenozoic lithoprobes and the loss of >120 km of Archean lithosphere, Sino-Korean craton, China. In *Magmatic Processes and Plate Tectonics*, vol. 76 (eds. H. M. Prichard, T. Alabaster, N. B. W. Harris and C. R. Neary). Geol Soc Spec Pub, pp. 71–81.

Menzies M. A. and Xu Y. G. (1998) Geodynamics of the North China Craton. In *Mantle Dynamics and Plate Interactions in East Asia*, vol. 27 (eds. M. F. J. Flower, S. L. Chung, C. H. Lo and T. Y. Lee), pp. 155–165. Geodynamics Series. the American Geophysical Union.

Morgan Z. and Liang Y. (2005) An experimental study of the kinetics of lherzolite reactive dissolution with applications to melt channel formation. *Contrib. Mineral. Petrol.* **150**(4), 369–385.

Mukhopadhyay S., Lassiter J. C., Farley K. A. and Bogue S. W. (2003) Geochemistry of Kauai shield-stage lavas: implications for the chemical evolution of the Hawaiian plume. *Geochem. Geophys. Geosyst.* **4**(1), 1009. doi:10.1029/2002GC000342.

Niu Y.-L. and Batiza R. (1997) Trace element evidence from seamounts for recycled oceanic crust in the Eastern Pacific mantle. *Earth Planet. Sci. Lett.* **148**, 471–483.

Niu Y. (2004) Bulk-rock major and trace element compositions of abyssal peridotites: implications for mantle melting, melt extraction and post-melting processes beneath mid-ocean ridges. *J. Petrol.* **45**(12), 2423–2458.

Niu Y. (2005) Generation and evolution of basaltic magmas: some basic concepts and a new view on the origin of Mesozoic–Cenozoic Basaltic Volcanism in Eastern China. *Geological J. China Universities* **11**(1), 9–46.

Niu Y., Regelous M., Wendt I. J., Batiza R. and O'Hara M. J. (2002) Geochemistry of near-EPR seamounts: importance of source vs. process and the origin of enriched mantle component. *Earth Planet. Sci. Lett.* **199**(3–4), 327–345.

Niu Y. L. and O'Hara M. L. (2003) Origin of ocean island basalts: a new perspective from petrology, geochemistry, and mineral physics considerations. *J. Geophys. Res.* **108**(B4), 2209. doi:10.1029/2002JB002048.

Norman M. D. and Garcia M. O. (1999) Primitive magmas and source characteristics of the Hawaiian plume: petrology and geochemistry of shield picrites. *Earth Planet. Sci. Lett.* **168**(1–2), 27–44.

Parman S. W. and Grove T. L. (2004) Harzburgite melting with and without H_2O: Experimental data and predictive modeling. *J. Geophys. Res.* **109**(B02201), 1–20.

Pearson D. G. and Nowell G. M. (2002) The continental lithospheric mantle: characteristics and significance as a mantle reservoir. *Phil. Trans. R. Soc. Lond. A* **360**, 2383–2410.

Pei F. P., Xu W. L., Wang Q. H., Wang D. Y. and Lin J. Q. (2004) Mesozoic basalt and mineral chemistry of the mantle-derived xenocrysts in Feixian, western Shandong, China: constraints on nature of Mesozoic lithospheric mantle. *Geological J. China Universities* **10**(1), 88–97.

Peng Z. C., Zartman R. E., Futa K. and Chen D. G. (1986) Pb-, Sr-, Nd-isotopic systematics, chemical characteristics of Cenozoic basalts, eastern China. *Chem. Geol.* **59**, 3–33.

Pertermann M. and Hirschmann M. M. (2003a) Anhydrous partial melting experiment on MORB-like eclogites phase relations, phase composition and mineral–melt partitioning of major elements at 2–3 GPa. *J. Petrol.* **44**, 2173–2202.

Pertermann M. and Hirschmann M. M. (2003b) Partial melting experiments on a MORB-like pyroxenite between 2 and 3 GPa: constraints on the presence of pyroxenites in basalt source regions. *J. Geophys. Res.* **108**(B2), 2125. doi:10.1029/2000JB000118.

Pertermann M., Hirschmann M. M., Hametner K., Günther D. and Schmidt M. W. (2004) Experimental determination of trace element partitioning between garnet and silica-rich liquid during anhydrous partial melting of MORB-like eclogite. *Geochem. Geophys. Geosyst.* **5**(Q05A01). doi:10.1029/2003GC000638.

Pfänder J. A., Münker C., Stracke A. and Mezger K. (2007) Nb/Ta and Zr/Hf in ocean island basalts—implications for crust–mantle differentiation and the fate of Niobium. *Earth Planet. Sci. Lett.* **254**(1–2), 158–172.

Pickering-Witter J. and Johnston A. D. (2000) The effects of variable bulk composition on the melting systematics of fertile peridotitic assemblage. *Contrib. Mineral. Petrol.* **140**, 190–211.

Rapp R. P., Shimizu N. and Norman M. D. (2003) Growth of early continental crust by partial melting of eclogite. *Nature* **425**, 605–609.

Rapp R. P., Shimizu N., Norman M. D. and Applegate G. S. (1999) Reaction between slab-derived melts and peridotite in the mantle wedge: experimental constraints at 3.8 GPa. *Chem. Geol.* **160**, 335–356.

Rapp R. P. and Watson E. B. (1995) Dehydration melting of metabasalt at 8–32 kbar: implications for continental growth and crust-mantle recycling. *J. Petrol.* **36**, 891–931.

Ringwood A. E. (1974) The petrological evolution of island arc systems. *J. Geol. Soc. London* **130**, 183–204.

Ringwood A. E. and Green D. H. (1966) An experimental investigation of the gabbro-eclogite transformation and some geophysical implications. *Tectonophysics* **3**(5), 383–427.

Rudnick R. L. (1995) Making continental crust. *Nature* **378**, 571–578.

Rudnick R. L., Barth M., Horn I. and McDonough W. F. (2000) Rutile-bearing refractory eclogites: missing link between continents and depleted mantle. *Science* **287**, 278–281.

Rudnick R. L. and Gao S. (2003) Composition of the continental crust. In *The Crust*, vol. 3 (ed. R. L. Rudnick). Elsevier, pp. 1–70.

Rudnick R. L., Gao S., Ling W. L., Liu Y. S. and McDonough W. F. (2004) Petrology and geochemistry of spinel peridotite xenoliths from Hannuoba and Qixia, North China craton. *Lithos* **77**(1–4), 609–637.

Ryerson F. J. and Watson E. B. (1987) Rutile saturation in magmas: implications for Ti–Nb–Ta depletion in island-arc basalts. *Earth Planet. Sci. Lett.* **86**(2–4), 225–239.

Salters V. and Stracke A. (2004) Composition of the depleted mantle. *Geochem. Geophys. Geosyst.* **5**(5), Q05004, 10.1029/2003GC000597.

Salters V. J. M. and Dick H. J. B. (2002) Mineralogy of the mid-ocean-ridge basalt source from neodymium isotopic composition of abyssal peridotites. *Nature* **418**, 68–72.

Scherstén A., Elliott T., Hawkesworth C. and Norman M. (2004) Tungsten isotope evidence that mantle plumes contain no contribution from the Earth's core. *Nature* **427**(6971), 234–237.

Schiano P., Eiler J., Hutcheon I. and Stolper E. (2000) Primitive CaO-rich, silica-undersaturated melts in island arcs: evidence for the involvement of clinopyroxene-rich lithologies in the petrogenesis of arc magmas. *Geochem. Geophys. Geosyst.*, 1999GC000032.

Schmidt M. W., Dardon A., Chazot G. and Vannucci R. (2004) The dependence of Nb and Ta rutile–melt partitioning on melt composition and Nb/Ta fractionation during subduction processes. *Earth Planet. Sci. Lett.* **226**(3–4), 415–432.

Schwab B. E. and Johnston A. D. (2001) Melting systematics of modally variable, compositionally intermediate peridotites and the effects of mineral fertility. *J. Petrol.* **42**(10), 1789–1811.

Sen C. and Dunn T. (1994) Dehydration melting of a basaltic composition amphibolite at 1.5 and 2.0 Gpa: implications for the origin of adakites. *Contrib. Mineral. Petrol.* **117**, 394–409.

Sigmarsson O. and Steinthorsson S. (2007) Origin of Icelandic basalts: a review of their petrology and geochemistry. *J. Geodyn.* **43**(1), 87–100.

Sobolev A. V., Hofmann A. W., Kuzmin D. V., Yaxley G. M., Arndt N. T., Chung S.-L., Danyushevsky L. V., Elliott T., Frey F. A., Garcia M. O., Gurenko A. A., Kamenetsky V. S., Kerr A. C., Krivolutskaya N. A., Matvienkov V. V., Nikogosian I. K., Rocholl A., Sigurdsson I. A., Sushchevskaya N. M. and Teklay M. (2007) The amount of recycled crust in sources of mantle-derived melts. *Science* **316**(5823), 412–417.

Sobolev A. V., Hofmann A. W., Sobolev S. V. and Nikogosian I. K. (2005) An olivine-free mantle source of Hawaiian shield basalts. *Nature* **434**(31), 590–597.

Song Y. and Frey F. A. (1989) Geochemistry of peridotite xenoliths in basalt from Hannuoba, Eastern China: implications for subcontinental mantle heterogeneity. *Geochim. Cosmochim. Acta* **53**(1), 97–113.

Song Y., Frey F. A. and Zhi X. C. (1990) Isotopic characteristics of Hannuoba basalts, eastern China: implications for their petrogenesis and the composition of subcontinental mantle. *Chem. Geol.* **85**, 35–52.

Stalder R., Foley S. F., Brey G. P. and Horn I. (1998) Mineral-aqueous fluid partitioning of trace elements at 900–1200 °C and 3.0–5.7 GPa: new experimental data for garnet, clinopyroxene, and rutile, and implications for mantle metasomatism. *Geochim. Cosmochim. Acta* **62**(10), 1781–1801.

Stracke A., Salters V. J. M. and Sims K. W. W. (1999) Assessing the presence of garnet–pyroxenite in the mantle sources of basalts through combined hafnium–neodymium–thorium isotope systematics. *Geochem. Geophys. Geosyst.* **1**. doi:10.1029/1999GC000013.

Taylor S. R. and McLennan S. M. (1985) *The continental crust: its composition and evolution*. Blackwell Scientific.

Thirlwall M. F., Gee M. A. M., Lowry D., Mattey D. P., Murton B. J. and Taylor R. N. (2006) Low [delta]18O in the Icelandic mantle and its origins: evidence from Reykjanes Ridge and Icelandic lavas. *Geochim. Cosmochim. Acta* **70**(4), 993–1019.

Thomas Find K., Kaj H., Folkmar H., Jens F., Reinhard W. and Dieter G.-S. (2006) Combined trace element and Pb–Nd–Sr–O isotope evidence for recycled oceanic crust (upper and lower) in the iceland mantle plume. *J. Petrol.* **47**(9), 1705–1749.

Tiepolo M., Vannucci R., Oberti R., Foley S., Bottazzi P. and Zanetti A. (2000) Nb and Ta incorporation and fractionation in titanian pargasite and kaersutite: crystal-chemical constraints and implications for natural systems. *Earth Planet. Sci. Lett.* **176**(2), 185–201.

Tuff J. and Gibson S. A. (2007) Trace-element partitioning between garnet, clinopyroxene and Fe-rich picritic melts at 3 to 7 GPa Contrib. *Mineral. Petrol.* **153**(4), 369–387.

Varfalvy V., Hebert R., Bedard J. and Lafleche M. (1997) Petrology and geochemistry of pyroxenite dykes in upper mantle peridotites of the North Arm Mountain massif, Bay of Islands ophiolite, Newfoundland: implications for the genesis of boninitic and related magmas. *Can. Mineral.* **35**(2), 543–570.

Walker D., Beattie P. and Jones J. H. (1992) Partitioning of U–Th–Pb and other incompatibles between augite and carbonate liquid at 1200 °C and 55 kbar. *EOS* **73**, 616.

Walter M. J. (1998) Melting of garnet peridotite and the origin of komatiite and depleted lithosphere. *J. Petrol.* **39**, 29–60.

Wang J. W. and Xie G. H. (1992) The geochemistry of Quaternary potassic lava in Wudalianci. In *The Age and Geochemistry of Cenozoic Volcanic Rock in China* (ed. R. X. Liu). Seismic Press, pp. 213–227.

Wang Q. H., Xu W. L., Wang D. Y., Lin J. Q. and Gao S. (2005) Geochemical characteristics of eclogite xenoliths in Mesozoic intrusive complex from Xu-Huai area and its tectonic significance. *Earth Sci. J. China University Geosci.* **30,** pp. 414–420 (in Chinese with English abs.).

Wang W., Xu W., Wang D., Ji W., Yang D. and Pei F. (2007) Caiyuanzi Paleogene basalts and deep-derived xenocrysts in eastern Liaoning, China: constraints on nature and deep process of the Cenozoic lithospheric mantle. *J. Mineral. Petrol.* **27**(1), 63–70.

Wang W., Xu W. L., Ji W. Q., Yang D. B. and Pei F. P. (2006) Late Mesozoic and Paleogene basalts and deep-derived xenocrysts in eastern Liaoning province, China: constraints on nature of lithospheric mantle. *Geological J. China Universities* **12**(1), 30–40.

Wasylenki L., Baker M., Kent A. and Stolper E. (2003) Near-solidus melting of the shallow upper mantle: partial melting experiments on depleted peridotite. *J. Petrol.* **44**(7), 1163–1191.

Wendlandt R. F. (1990) Partitioning of niobium and tantalum between rutile and silicate melt. *EOS* **71**, 1658.

Weyer S., Münker C. and Mezger K. (2003) Nb/Ta, Zr/Hf and REE in the depleted mantle: implications for the differentiation history of the crust–mantle system. *Earth Planet. Sci. Lett.* **205**, 309–324.

Wu F.-Y., Walker R. J., Yang Y.-H., Yuan H.-L. and Yang J.-H. (2006) The chemical-temporal evolution of lithospheric mantle underlying the North China Craton. *Geochim. Cosmochim. Acta* **70**(19), 5013–5034.

Wu F. Y., Lin J. Q., Wilde S. A., Zhang X. O. and Yang J. H. (2005) Nature and significance of the Early Cretaceous giant igneous event in eastern China. *Earth Planet. Sci. Lett.* **233**, 103–119.

Wu F. Y., Walker R. J., Ren X. W., Sun D. Y. and Zhou X. H. (2003) Osmium isotopic constraints on the age of lithospheric mantle beneath northeastern China. *Chem. Geol.* **196**, 107–129.

Xie G. H. and Wang J. W. (1992) The geochemistry of Cenozoic volcanic rock in the Changbaishan area. In *The Age and Geochemistry of Cenozoic Volcanic Rock in China* (ed. R. X. Liu). Seismic Press, pp. 210–212.

Xie X., Xu X., Zou H. and Xing G. (2001) Trace element and Nd–Sr–Pb isotope studies of Mesozoic and Cenozoic basalts in coastal area of SE China. *Acta Petrol. Sin. (in Chinese with English Abs.)* **17**(4), 617–628.

Xiong X. L. (2006) Trace element evidence for growth of early continental crust by melting of rutile-bearing hydrous eclogite. *Geology* **34**, 945–948.

Xiong X. L., Adam T. J. and Green T. H. (2005) Rutile stability and rutile/melt HFSE partitioning during partial melting of hydrous basalt: implications for TTG genesis. *Chem. Geol.* **218**, 339–359.

Xu J., Chen Y. C., Wang D. H., Yu J. J., Li C. J., Fu X. J. and Chen Z. Y. (2004) Titanium mineralization in the ultrahigh-pressure metamorphic rocks from Chinese Continental Scientific Drilling 100–2000 m main hole. *Acta Petrol. Sin. (in Chinese with English Abs.)* **20**(1), 119–126.

Xu J. F., Shinjo R., Defant M. J., Wang Q. and Rapp R. P. (2002) Origin of Mesozoic adakitic intrusive rocks in the Ningzhen area of east China: partial melting of delaminated lower continental crust? *Geology* **30**(12), 1111–1114.

Xu W., Hergt J. M., Gao S., Pei F., Wang W. and Yang D. (2008) Interaction of adakitic melt–peridotite: implications for the

high-Mg# signature of Mesozoic adakitic rocks in the eastern North China Craton. *Earth Planet. Sci. Lett.* **265**(1–2), 123–137.

Xu W. L., Gao S., Wang Q. H., Wang D. Y. and Liu Y. S. (2006) Mesozoic crustal thickening of the eastern North China craton: evidence from eclogite xenoliths and petrologic implications. *Geology* **34**(9), 721–724.

Xu W. L., Wang D. Y., Wang Q. H. and Lin J. Q. (2003) Petrology and geochemistry of two types of mantle-derived xenoliths in Mesozoic diorite from western Shandong province. *Acta Petrol. Sin.* **19**(4), 623–636.

Xu X. and Xie X. (2005) Late Mesozoic–Cenozoic basaltic rocks and crust–mantle interaction, SE China. *Geological J. China Universities* **11**(3), 318–334.

Xu Y.-G., Ma J.-L., Frey F. A., Feigenson M. D. and Liu J.-F. (2005) Role of lithosphere–asthenosphere interaction in the genesis of Quaternary alkali and tholeiitic basalts from Datong, western North China Craton. *Chem. Geol.* **224**(4), 247–271.

Xu Y. G. (2001) Thermo-tectonic destruction of the Archaean lithospheric keel beneath the Sino-Korean craton in China: evidence, timing and mechanism. *Phys. Chem. Earth (A)* **26**(9–10), 747–757.

Yan J., Chen J. F., Xie Z., Gao T. S., Foland K. A., Zhang X. D. and Liu M. W. (2005) Studies on petrology and geochemistry of the Later Cretaceous basalts and mantle-derived xenoliths from eastern Shandong. *Acta Petrol. Sin. (in Chinese with English Abs.)* **21**(1), 99–112.

Yang J. H., Chung S. L., Zha M. G. and Zhou X. H. (2004) Geochemical and Sr–Nd–Pb isotopic compositions of mafic dikes from the Jiaodong Peninsula, China: evidence for vein-plus-peridotite melting in the lithospheric mantle. *Lithos* **73**, 145–160.

Yasuda A., Fujii T. and Kurita K. (1994) Melting phase relations of an anhydrous mid-ocean ridge basalt from 3 to 20 GPa: implications for the behaviour of subducted oceanic crust in the mantle. *J. Geophys. Res.* **99**, 9401–9414.

Yaxley G. M. (2000) Experimental study of the phase and melting relations of homogeneous basalt + peridotite mixtures and implications for the petrogenesis of flood basalts. *Contrib. Mineral. Petrol.* **139**, 326–338.

Yaxley G. M. and Green D. H. (1998) Reactions between eclogite and peridotite: mantle refertilisation by subduction of oceanic crust. *Schweiz. Mineral. Petrogr. Mitt.* **78**, 243–255.

Yogodzinski G. M., Kay R. W., Volynets O. N., Koloskov A. V. and Kay S. M. (1995) Magnesian andesite in the western Aleutian Komandorsky region: implications for slab melting and processes in the mantle wedge. *GSA Bulletin* **107**(5), 505–519.

Yuan X., Sobolev S. V., Kind R., Oncken O., Bock G., Asch G., Schurr B., Graeber F., Rudloff A., Hanka W., Wylegalla K., Tibi R., Haberland C., Rietbrock A., Giese P., Wigger P., Rower P., Zandt G., Beck S., Wallace T., Pardo M. and Comte D. (2000) Subduction and collision processes in the Central Andes constrained by converted seismic phases. *Nature* **408**(6815), 958–961.

Zack T., Kronz A., Foley S. F. and Rivers T. (2002) Trace element abundances in rutiles from eclogites and associated garnet mica schists. *Chem. Geol.* **184**, 97–122.

Zanetti A., Tiepolo M., Oberti R. and Vannucci R. (2004) Trace-element partitioning in olivine: modelling of a complete dataset from a synthetic hydrous basanite melt. *Lithos* **75**, 39–54.

Zhang H. F., Sun M., Zhou M. F., Fan W. M., Zhou X. H. and Zhai M. G. (2004) Highly heterogeneous Late Mesozoic lithospheric mantle beneath the North China Craton: evidence from Sr–Nd–Pb isotopic systematics of mafic igneous rocks. *Geol. Mag.* **141**, 55–62.

Zhang H. F., Sun M., Zhou X. H., Fan W. M., Zhai M. G. and Yin J. F. (2002) Mesozoic lithosphere destruction beneath the North China Craton: evidence from major-, trace-element and Sr–Nd–Pb isotope studies of Fangcheng basalts. *Contrib. Mineral. Petrol.* **144**, 241–253.

Zhang H. F., Sun M., Zhou X. H., Zhou M. F., Fan W. M. and Zheng J. P. (2003) Secular evolution of the lithosphere beneath the eastern North China Craton: evidence from Mesozoic basalts and high-Mg andesites Geochim. *Cosmochim. Acta* **67**, 4373–4387.

Zhang H. F. and Zheng J. P. (2003) Geochemical characteristics and petrogenesis of Mesozoic basalts from the North China Craton: a case study in Fuxin, Liaoning Province. *Chin. Sci. Bull.* **48**(9), 924–930.

Zhang J. B. and Chen D. G. (1992) The geochemistry of basalt in the two areas of Longhai and Mingxi in Fujian Province. In *The age and geochemistry of Cenozoic volcanic rock in China* (ed. R. X. Liu). Seismic Press, pp. 298–319.

Zhang M., Tu K., Xie G. H., Flower M. F. J. and Carlson R. W. (1992) The trace element and isotope geochemistry of Cenozoic basalt in Hainan island. In *The age and geochemistry of Cenozoic volcanic rock in China* (ed. R. X. Liu). Seismic Press, pp. 246–268.

Zhang M., Zhou X.-H. and Zhang J.-B. (1998) Nature of the lithospheric mantle beneath NE China: evidence from potassic volcanic rocks and mantle xenoliths. In *Mantle Dynamics and Plate Interactions in East Asia*, vol. 27 (eds. M. F. J. Flower, S.-L. Chung, C.-H. Lo and T.-Y. Lee). American Geophysical Union Geodynamics Series, pp. 197–220.

Zhang Z. M., Xu Z. Q. and Xu H. F. (2000) Petrology of ultrahigh-pressure eclogites from the ZK703 drillhole in the Donghai, eastern China. *Lithos* **52**, 35–50.

Zhao G. C., Cawood P. A., Wilde S. A., Sun M. and Lu L. Z. (2000) Metamorphism of basement rocks in the Central Zone of the North China Craton: implications for Paleoproterozoic tectonic evolution. *Precambrian Res.* **103**, 55–88.

Zheng J. P., Griffin W. L., O'Reilly S. Y., Lu F. X., Wang C. Y., Zhang M., Wang F. Z. and Li H. M. (2004) 3.6 Ga lower crust in central China: new evidence on the assembly of the North China craton. *Geology* **32**(3), 229–232.

Zhi X., Song Y., Frey F. A., Feng J. and Zhai M. (1990) Geochemistry of Hannuoba basalts, eastern China: constraints on the origin of continental alkalic and tholeiitic basalt. *Chem. Geol.* **88**(1–2), 1–33.

Zhi X. C. and Feng J. L. (1992) The geochemistry of basalt in Hannuoba. In *The Age and Geochemistry of Cenozoic Volcanic Rock in China* (ed. R. X. Liu). Seismic Press, pp. 114–148.

Zhou X., Sun M., Zhang G. and Chen S. (2002) Continental crust and lithospheric mantle interaction beneath North China: isotopic evidence from granulite xenoliths in Hannuoba, Sino-Korean craton. *Lithos* **62**(3–4), 111–124.

Zhou X., Zhang G., Yang J. and Chen W. M S. (2001) Sr–Nd–Pb isotope mapping of Late Mesozoic volcanic rocks across northern margin of North China Craton and implications to geodynamic processes. *Geochimica* **30**(1), 10–23.

Zhou X. H. and Armstrong R. L. (1982) Cenozoic volcanic rocks of eastern China: secular and geographic trends in chemistry and strontium isotopic composition Earth Planet. *Sci. Lett.* **58**, 301–329.

Zhou X. H., Zhou H. L. E M. L., Zhang J. P. and Cheng H. (1992) The discovery of continuous transition series of Mesozoic–Cenozoic hidden basalt in the Shanghai area and its geochemical genesis study. In *The Gge and Geochemistry of Cenozoic Volcanic Rock in China* (ed. R. X. Liu). Seismic Press, pp. 285–296.

Zhou Z., Barrett P. M. and Hilton J. (2003) An exceptionally preserved Lower Cretaceous ecosystem. *Nature* **421**, 807–814.

Zou H. B., Zindler A., Xu X. S. and Qi Q. (2000) Major, trace element, and Nd, Sr and Pb isotope studies of Cenozoic basalts in SE China: mantle sources, regional variations, and tectonic significance. *Chem. Geol.* **171**, 33–47.

Associate editor: Martin A. Menzies